

AD-A193 846

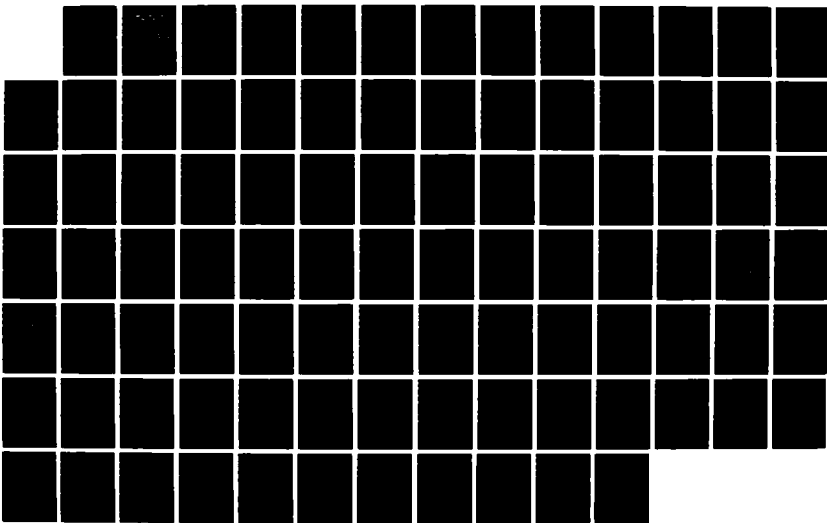
PROBABILISTIC ANISOTROPIC FAILURE CRITERIA FOR
COMPOSITE MATERIALS(U) NAVAL POSTGRADUATE SCHOOL
MONTEREY CA K J NELSON DEC 87

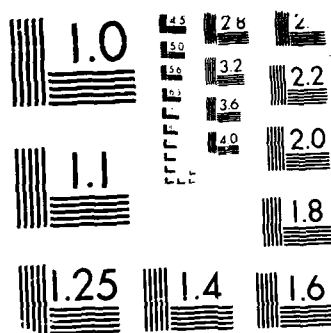
171

UNCLASSIFIED

F/G 11/4

NL





MICROCOPY RESOLUTION TEST CHART

U.S. GOVERNMENT PRINTING OFFICE: 1963 O

DTIC FILE COPY

2

NAVAL POSTGRADUATE SCHOOL Monterey, California

AD-A193 046



THESIS

DTIC
ELECTE
JUN 06 1988
S H D

PROBABILISTIC ANISOTROPIC FAILURE CRITERIA FOR COMPOSITE MATERIALS

by

Kenneth John Nelson

December 1987

Thesis Advisor:

Edward M. Wu

Approved for public release; distribution is unlimited.

UNCLASSIFIED

SECURITY CLASSIFICATION OF THIS PAGE

REPORT DOCUMENTATION PAGE				
1a REPORT SECURITY CLASSIFICATION UNCLASSIFIED		1b RESTRICTIVE MARKINGS		
2a SECURITY CLASSIFICATION AUTHORITY		3 DISTRIBUTION/AVAILABILITY OF REPORT Approved for Public Release; Distribution Unlimited		
2b DECLASSIFICATION/DOWNGRADING SCHEDULE				
4 PERFORMING ORGANIZATION REPORT NUMBER(S)		5 MONITORING ORGANIZATION REPORT NUMBER(S)		
6a NAME OF PERFORMING ORGANIZATION Naval Postgraduate School	6b OFFICE SYMBOL (if applicable) 67	7a NAME OF MONITORING ORGANIZATION Naval Postgraduate School		
6c ADDRESS (City, State, and ZIP Code) Monterey, California 93943-5000		7b ADDRESS (City, State, and ZIP Code) Monterey, California 93943-5000		
8a NAME OF FUNDING/SPONSORING ORGANIZATION	8b OFFICE SYMBOL (if applicable)	9 PROCUREMENT INSTRUMENT IDENTIFICATION NUMBER		
8c ADDRESS (City, State, and ZIP Code)		10 SOURCE OF FUNDING NUMBERS		
		PROGRAM ELEMENT NO	PROJECT NO	TASK NO
		WORK UNIT ACCESSION NO		
11 TITLE (Include Security Classification) PROBABILISTIC ANISOTROPIC FAILURE CRITERIA FOR COMPOSITE MATERIALS				
12 PERSONAL AUTHOR(S) Nelson, Kenneth John				
13a TYPE OF REPORT Master's Thesis	13b TIME COVERED FROM TO	14 DATE OF REPORT (Year, Month, Day) 1987 December	15 PAGE COUNT 91	
16 SUPPLEMENTARY NOTES				
17 COSATI CODES		18 SUBJECT TERMS (Continue on reverse if necessary and identify by block number)		
FIELD	GROUP	SUB-GROUP		
			Failure criterion, failure envelope, composite material probability	
19 ABSTRACT (Continue on reverse if necessary and identify by block number)				
<p>A most important structural design objective today is the reliable applications of composite materials. Reliability is associated with the probability of success or failure of a particular structure and/or composite material. For this study, the reliability associated with strength was investigated.</p> <p>The objective was to develop a probabilistic anisotropic failure criterion and an analytical model which would account for the inherent strength scatter and enhance the structural reliability phase of composite design. This study analytically described the failure criterion and probabilistic failure states of a anisotropic composite in a combined stress state. Strength sensitivity and the failure mechanism within the domain of the combined stress space was based on a numerical simulation of a theoretical mathematical model.</p>				
20 DISTRIBUTION/AVAILABILITY OF ABSTRACT <input checked="" type="checkbox"/> UNCLASSIFIED/UNLIMITED <input type="checkbox"/> SAME AS RPT <input type="checkbox"/> DTIC USERS		21 ABSTRACT SECURITY CLASSIFICATION UNCLASSIFIED		
22a NAME OF RESPONSIBLE INDIVIDUAL Professor Edward M. Whi		22b TELEPHONE (Include Area Code) (408) 646 2452	22c OFFICE SYMBOL 67W1	

UNCLASSIFIED

SECURITY CLASSIFICATION OF THIS PAGE (When Data Entered)

(19. continued)

The numerical simulation was analogous to physical testing of large composite sample sizes.

For the probabilistic and mechanistic independent case examined, the failure envelopes as defined by the failure criterion exhibited a mechanistic dependent phenomenological appearance. The size and shape of the resulting phenomenological failure envelopes were dependent on the intrinsic shape parameters and their combinations associated with the longitudinal strength and transverse strength. The probabilistic formulation of the failure criterion could reconcile the difference between the phenomenologically coupled and the uncoupled failure criterion. In addition, the probabilistic failure criterion would provide analytical guidance for definitive experimental measurements. Finally, the probabilistic failure criterion would provide the analytical conditions for optimal design and feedback in composite material development and quality assurance.



Accession For	
NTIS GRA&I	<input checked="" type="checkbox"/>
DTIC TAB	<input type="checkbox"/>
Unannounced	<input type="checkbox"/>
Justification	
By	
Distribution/	
Availability Codes	
Dist	Avail and/or Special
A-1	

S N 0102- LF 014- 6601

UNCLASSIFIED

SECURITY CLASSIFICATION OF THIS PAGE(When Data Entered)

Approved for public release; distribution is unlimited.

**Probabilistic Anisotropic Failure Criteria
For Composite Materials**

by

Kenneth John Nelson
Lieutenant Commander, United States Navy
M.B.A., George Washington University, 1983

Submitted in partial fulfillment of the
requirements for the degree of

MASTER OF SCIENCE IN AERONAUTICAL ENGINEERING

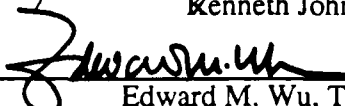
from the

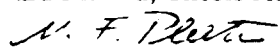
**NAVAL POSTGRADUATE SCHOOL
December 1987**

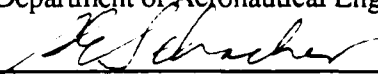
Author:


Kenneth John Nelson

Approved by:


Edward M. Wu, Thesis Advisor


M. F. Platzer, Chairman,
Department of Aeronautical Engineering


G. E. Schacher
Dean of Science and Engineering

ABSTRACT

A most important structural design objective today is the reliable applications of composite materials. Reliability is associated with the probability of success or failure of a particular structure and/or composite material. For this study, the reliability associated with strength was investigated.

The objective was to develop a probabilistic anisotropic failure criterion and an analytical model which would account for the inherent strength scatter and enhance the structural reliability phase of composite design. This study analytically described the failure criterion and probabilistic failure states of a anisotropic composite in a combined stress state. Strength sensitivity and the failure mechanism within the domain of the combined stress space was based on a numerical simulation of a theoretical mathematical model. The numerical simulation was analogous to physical testing of large composite sample sizes.

For the probabilistic and mechanistic independent case examined, the failure envelopes as defined by the failure criterion exhibited a mechanistic dependent phenomenological appearance. The size and shape of the resulting phenomenological failure envelopes were dependent on the intrinsic shape parameters and their combinations associated with the longitudinal strength and transverse strength. The probabilistic formulation of the failure criterion could reconcile the difference between the phenomenologically coupled and the uncoupled failure criterion. In addition, the probabilistic failure criterion would provide analytical guidance for definitive experimental measurements. Finally, the probabilistic failure criterion would provide the analytical conditions for optimal design and feedback in composite material development and quality assurance.

TABLE OF CONTENTS

I. INTRODUCTION	11
II. BACKGROUND	14
III. NUMERICAL SIMULATION	18
A. CHANGES IN THE SHAPE PARAMETER (α)	19
B. THEORETICAL MATHEMATICAL MODEL	22
C. BIAXIAL L/T NUMERICAL SIMULATION	23
IV. RESULTS	24
A. BIAXIAL L/T NUMERICAL SIMULATION	24
B. ANALYTICAL EVALUATION OF MODEL	30
V. CONCLUSIONS AND RECOMMENDATIONS	45
APPENDIX A THEORETICAL MATHEMATICAL MODEL	46
APPENDIX B BIAXIAL L/T NUMERICAL SIMULATION	50
APPENDIX C NUMERICAL SIMULATION FORMULATION	55
APPENDIX D GAUSS QUADRATURE MEAN STRENGTH INTEGRATION	64
APPENDIX E SIMULATION/MODEL MEAN STRENGTH WORKSHEET	69
APPENDIX F RELIABILITY/FAILURE FUNCTION WORKSHEET	76
APPENDIX G PERCENTILE STRENGTH WORKSHEET	80
LIST OF REFERENCES	88
BIBLIOGRAPHY	90
INITIAL DISTRIBUTION LIST	91

LIST OF FIGURES

1	PDF—Normalized $\theta=0$	19
2	PDF—Normalized $\theta=0$	20
3	PDF—Normalized $\theta=45$	21
4	PDF—Normalized $\theta=45$	21
5	Intrinsic Strength Space $\theta=45$	24
6	Realized Strength Space $\theta=45$	25
7	Realized Strength Space $\theta=45$	25
8	Realized Strength Space $\theta=45$	26
9	Realized Strength Space $\theta=10, 30, 45, 60, 80$	27
10	Relative Frequency Strength Space $\theta=45$	28
11	Joint Probability Strength Space $\theta=45$	28
12	Failure Envelope or Failure Surface	29
13	Failure Envelope or Failure Surface	30
14	Failure Function $\alpha_1=60, \alpha_2=5$	31
15	Failure Function $\alpha_1=60, \alpha_2=5$	31
16	Failure Function $\alpha_1=60, \alpha_2=5$	32
17	Reliability Function $\alpha_1=60, \alpha_2=5$	32
18	Relative Frequency Strength Space $\theta=45$	33
19	Relative Frequency Strength Space $\theta=45$	34

20	Failure Envelope or Failure Surface	35
21	Failure Envelope or Failure Surface	35
22	Failure Envelope or Failure Surface	36
23	Failure Envelope or Failure Surface	36
24	Failure Function $\alpha_1=60, \alpha_2=5, \theta=55$	37
25	Failure Function $\alpha_1=60, \alpha_2=5, \theta=48$	38
26	Failure Function $\alpha_1=60, \alpha_2=5, \theta=42$	38
27	Failure Function $\alpha_1=60, \alpha_2=5, \theta=35$	39
28	Failure Function $\alpha_1=60, \alpha_2=5, \theta=30$	39
29	Failure Function $\alpha_1=60, \alpha_2=60, \theta=45$	41
30	Failure Function $\alpha_1=20, \alpha_2=5, \theta=45$	41
31	Failure Function $\alpha_1=5, \alpha_2=5, \theta=45$	42
32	Failure Envelope or Failure Surface	43
33	Failure Envelope or Failure Surface	43
34	Applied Stress Ratio in Normalized Domain	46
35	Applied Stress Ratio in Physical Domain	47
36	Applied Stress Ratio in Normalized Domain	50
37	Applied Stress Ratio in Physical Domain	51
38	Composite Fails by Fiber	52
39	Composite Fails by Matrix	53
40	Joint Probability (Independent) Realized Strength Space	54

LIST OF SYMBOLS

α_1, α_2	Longitudinal and transverse shape parameters respectively
A1, A2	Longitudinal and transverse shape parameters respectively
Alfa1, Alfa2	Longitudinal and transverse shape parameters respectively
β_1, β_2	Longitudinal and transverse scale parameters respectively
B1, B2	Longitudinal and transverse scale parameters respectively
Beta1, Beta2	Longitudinal and transverse scale parameters respectively
Biaxial L/T	Applied stress biaxial ratio
F	Expected Rank
f()	Density of the probability failure function F()
F()	Probability failure function
F1(), F2()	Failure function components associated with the longitudinal and transverse failure modes respectively
F*	Weibull probability function
L	Longitudinal strength or stress
μ	Mean strength
$\mu(0), \mu(90)$	Mean strength at normalized (uniaxial) zero (0) and ninety (90) degree radial loading paths respectively
R()	Probability reliability function
R1(), R2()	Reliability function components associated with the longitudinal and transverse failure modes respectively

σ	Stress
σ_1, σ_2	Normal stress components along the longitudinal and transverse directions respectively
S	Strength vector
T	Transverse strength or stress
Theta	Applied stress ratio
θ	Applied stress ratio
X	Intrinsic strength vector
X1, X2	Strength components along the longitudinal and transverse directions respectively

ACKNOWLEDGMENTS

To my wife, Nancy, and our two children, Kate and Beau, for their everlasting support, happiness, and love. To Mr. Jim Nageotte for his administrative support. To Professor D. G. Harlow of Lehigh University, Pennsylvania for his expertise on probability modeling.

To Professor Edward M. Wu for his total dedication to this study and his unique outlook on life and education. He is a person for whom I have great respect and admiration. I applaud his accomplishments and his contributions to our country.

I. INTRODUCTION

One important structural design objective today is the reliable applications of composite materials. With respect to structural design, a first phase may establish the design mission requirements, i.e., the strength and stiffness requirements of a particular composite material. A second phase may determine the optimal composite material based on the design requirements and trade-offs, i.e., the benefits and costs associated with a particular composite material. A third phase may determine the optimal lamination configuration by tailoring a particular composite, i.e., volume fraction of fiber and matrix, ply angles, number of plies and ply groups. A forth phase may determine the structural reliability of a particular composite. The structural design reliability phase was characterized by evaluating the optimal structural stress or strength levels for an acceptable number of probable successes or failures. Reliability was associated with probability where structural performance and quality assurance were measured by the probability of success or failure of a particular structure and/or composite material. The objective of this study was to develop a analytical model for probabilistic anisotropic failure criterion which would account for the inherent strength scatter (directional dependence) and quantify the structural reliability phase of composite design.

The reliability of a structure would be quantitatively evaluated by examining the state of stress at every spatial location against the magnitude of the failure state as defined by the failure criterion. Mathematically, this consisted of mapping of a stress tensor associated with the spatial domain of a particular structure into a failure domain. Operationally, the spatial distribution of the stress state in a particular structure would be obtained by an appropriate branch of stress analysis (elasticity, viscoelasticity, plasticity, etc.), which were frequently implemented with many finite element analysis computer codes. The evaluation

of (proximity to) the failure state required a theoretical mathematical model of the failure state (as defined by the failure criterion). Many failure criterion have been proposed for different materials (isotropic and anisotropic, crystalline and amorphous, and homogeneous and nonhomogeneous composites) with different failure modes (yielding and brittle failure). These failure criteria may be mechanistically or phenomenologically based.

This study analytically described the failure criterion and failure states of a probabilistic anisotropic composite and was based on numerical simulations of a theoretical mathematical model. Four domains (physical, stress, failure, and normalized) were defined in this study in order to describe the spatial location of a particular structure in a prescribed space. In a physical domain, each spatial location of a particular structure was associated with a second rank stress tensor (σ_{ij}) which had nine (9) scalar stress components on three (3) orthogonal planes and was a function of coordinate orientation. It was cumbersome to represent a tensor higher than the first rank tensor in the failure domain. For simplicity and without loss of generality, the physical domain in this study was restricted to:

each spatial location was associated with a second rank stress tensor (σ_{ij}) which only had two non-zero scalar normal stress components (σ_1, σ_2) on one plane. [Ref. 1]

Furthermore, numerical investigations were confined to the first quadrant in order to define this normal stress domain. The stress domain was defined as a biaxial normal stress state (σ_1, σ_2) with both the longitudinal stress in tension and the transverse stress in tension.

With the restriction that the shear stress components were zero, the magnitude of the normal stresses at each spatial location of a particular structure was mapped into a respective point on the biaxial stress space. If all the stress points were interior to the domain bounded by a strength distribution (failure envelope), then the entire structure was

safe ($0 \leq \sigma_i \leq X_i$). If any of the stress points were exterior to the domain bounded by a strength distribution (failure envelope), then the corresponding spatial location of a particular structure was not safe (failed with $\sigma_i > X_i$). If the structure was monolithic (single element), then the entire structure failed. If the structure was redundant (load sharing), then failure at a spatial location increased the probability of failure of the entire structure. This condition would not cause the direct failure of the entire structure. [Ref. 2]

The failure domain (failure criteria) was described by the failure envelope or failure surface in the biaxial stress domain and was expressed for this study by a mean strength contour and a percentile strength contour. The failure domain was presented to identify the parametric role of the variability in the longitudinal and transverse strength on the size and shape of the failure criterion. The normalized domain was used as a radial loading path transition to the biaxial stress domain.

II. BACKGROUND

One of the primary objectives of composite design is to capitalize on the high strength and stiffness-to-weight ratios, which are important attributes of composite materials. A composite is made of two or more woven or nonwoven constituent materials which are fiber-reinforced in a matrix. A fiber is a single filament which is formed in one direction (unidirectional). Matrix binds the filaments to form a composite material. [Ref. 3]

Fibers are the principal reinforcing or load carrying agent of a composite material. The primary function of matrix is to support and protect the fibers, to provide a load distribution or load sharing mechanism for a weak fiber, and to provide micro-redundancy within a composite material. [Ref. 4]

A frequently occurring consequence of composite materials is that the physical properties of the resulting materials become highly anisotropic [Ref. 5]. An anisotropic composite exhibits material properties that vary with orientation or direction of the reference coordinate system [Ref. 6].

Failure characterization of composites is defined by the level of observation. A phenomenological approach may be used to address the probabilistic anisotropic failure criteria for composite materials. The phenomenological approach treats the heterogeneous composites as a continuum, and an analytical model is used to correlate the occurrence of the material responses without necessarily explaining the mechanisms which lead to these material responses. The incorporation of probabilistic phenomena in failure criterion will provide the ground work for the mechanistic understanding of the interacting failure mechanisms. The failure characterization of anisotropic composites will be treated herein in accordance with the fundamentals of the phenomenological approach, where: (1) conduct a numerical simulation of the theoretical model, which is analogous to physical testing of

numerous composite samples, and (2) evaluate and interpret the results of the numerical simulation and infer the definitive experiments. The phenomenological approach is intended to aid experimental design; to facilitate interpolation, correlation, and retrieval of experimental observations; and may be valuable for identifying definitive experiments to quantitatively measure the mechanisms for failure. [Ref. 7]

Failure criterion is an analytical description of the failure states of a composite material subjected to a complex state of stresses or strains [Ref. 8]. Failure criterion may be geometrically interpreted as a limiting envelope in the stress space, i.e., the condition for composite failure occurs when a given stress vector penetrates the failure envelope or failure surface [Ref. 9]. In other words, the failure envelope or failure surface is the ultimate limit (lower bound-worst case) for a combined stress or strain state as defined by the failure criterion [Ref. 10]. Taking into account the statistical scatter, the analytical structure of the failure envelope or failure surface was the objective of this study.

In the development of probabilistic anisotropic failure criteria model for composite materials, the primary theoretical basis of this study in the biaxial stress domain was on the two parameter Weibull model for the uniaxial longitudinal and transverse stress states and the resulting joint probability distribution function for the combined longitudinal and transverse stress states. The two parameter Weibull distribution and the joint probability distribution were expressed as a function of the applied stress ratio radial loading path in the two dimensional biaxial stress domain (σ_1, σ_2). The Weibull distribution function was characterized by an unimodal distribution and the joint probability distribution function was characterized by an unimodal or bimodal distribution.

The combined stress state explored the statistical and mechanistic contributions of the probabilistic independent and mechanistic independent case. Joint probability for this study was defined as the intrinsic strength which was activated by the stress (σ_1) in the

longitudinal or fiber direction is independent of the intrinsic strength which was activated by the stress (σ_2) in the transverse or matrix direction. The strengths were uncoupled and the failure mechanisms were not interacting. [Ref. 11]

Mechanistic independence for this study was defined as a stress activated mechanism where the stress components (σ_1 and σ_2) are independent. The corresponding failure mechanism in the strain space was coupled through the stress/strain constitutive relationship ($\epsilon_{ij} = S_{ijkl}\sigma_{kl}$). In this relationship stress was the independent variable and strain was the dependent variable.

The two-parameter Weibull distribution was based on the reliability function $R(X)$ and was defined for this study as:

$$R(X) = 1 - F(X)$$

where:

- (1) $R(X)$ was the Weibull distribution reliability function.
- (2) $F(X)$ was the Weibull distribution failure function.
- (3) $R_1(X_1) = \exp(-(X_1/\beta_1)^{\alpha_1})$. The reliability function in the uniaxial longitudinal or fiber direction.
- (4) $R_2(X_2) = \exp(-(X_2/\beta_2)^{\alpha_2})$. The reliability function in the uniaxial transverse or matrix direction.
- (5) X_1 and X_2 were the random intrinsic strengths in the uniaxial longitudinal and transverse directions.
- (6) α_1 and β_1 were the Weibull shape and scale parameters in the uniaxial longitudinal or fiber direction.
- (7) α_2 and β_2 were the Weibull shape and scale parameters in the uniaxial transverse or matrix direction. [Ref. 12]

As a result of joint probability (independence) assumption for the combined stress states, the joint probability function was based on the Weibull reliability functions in the

uniaxial longitudinal and transverse directions respectively and for this study was defined as:

$$R(X) = R_1(X_1) * R_2(X_2)$$

where:

- (1) $R(X) = \exp [-(X_1/\beta_1)^{\alpha_1} + (X_2/\beta_2)^{\alpha_2}]$
- (2) $F(X) = 1 - R(X) = 1 - \exp [-(X_1/\beta_1)^{\alpha_1} + (X_2/\beta_2)^{\alpha_2}]$
- (3) $R(X)$ was the reliability function and was equivalent to the probability of success associated with the random variables X_1 and X_2 .
- (4) $F(X)$ was the failure function and was equivalent to the probability of failure associated with the random variables X_1 and X_2 .
- (5) X_1 was the random intrinsic stress or strength in the longitudinal or fiber direction.
- (6) X_2 was the random intrinsic stress or strength in the transverse or matrix direction.
- (7) α_1 and β_1 were the joint probability shape (A1 or alfa1) and scale (B1 or beta1) parameters respectively in the longitudinal or fiber direction.
- (8) α_2 and β_2 were the joint probability shape (A2 or alfa2) and scale (B2 or beta2) parameters respectively in the transverse or matrix direction.

The joint probability failure envelope or failure surface of the failure criterion model was represented for this study by a mean failure surface and a percentile failure surface. The mean failure surface was the mean strength at which a number of samples failed for a particular applied stress ratio. The percentile failure surface was the fraction of samples which failed for a particular applied stress ratio. With respect to the intrinsic strengths, this study explored the dependency of the mean and percentile failure envelopes on the shape parameters (α_1 and α_2). The shape parameters were expressed as a function of the combined stress state.

III. NUMERICAL SIMULATION

Material failure involves numerous complex processes, many simplifications were unavoidable in the mathematical formulation of failure states and failure criteria. The assessment of those underlying simplifying assumptions would only be made through comparison with experimental data. Experimental measurements and data collection were very difficult for the evaluation of the combined stress states and the enormous number of different stress ratios that were required to cover the entire six-dimensional (6-D) stress space. As it was impractical for the overall verification of the entire failure domain, one must focus verifications at selected critical states. Numerical simulations may be used to deduce the consequences of the proposed models and as a comparison to identify regions where the predictions by different models were large.

Appendix A and B described the development of the theoretical mathematical model and the biaxial L/T numerical simulation respectively. The objective of this study was to develop probabilistic anisotropic failure criteria for composites. The failure criterion model for this study was defined as a function of the applied stress ratio and the joint probability distribution function scale (β_1 and β_2) and shape (α_1 and α_2) parameters. The initial conditions for the theoretical mathematical model and biaxial L/T numerical simulation were:

- (1) sample size = 199.
- (2) scale parameters $\beta_1 = 100$ and $\beta_2 = 1$.
- (3) shape parameters $\alpha_1 = 60$ and $\alpha_2 = 5$.
- (4) seventeen (17) applied stress ratios in the physical domain were based on the transformed theta in the normalized domain and were equivalent to: 0, 10, 20, 30, 35, 39, 42, 44, 45, 46, 48, 51, 55, 60, 70, 80, and 90 degree radial loading paths.

A. CHANGES IN THE SHAPE PARAMETER

This study evaluated the effect of various high ($\alpha_{1,2} = 60$) and low ($\alpha_{1,2} = 5$) combinations of the uniaxial shape parameters (α_1 and α_2) on the joint probability function. The scale parameters (β_1 and β_2) were fixed for this study.

The Coefficient of Variation (C.V.) is approximately equal to 1.2 divided by the shape parameter (α) [Ref. 13]. As a result, high shape parameter values were equivalent to low dispersion or scatter, and low shape parameter values were equivalent to high dispersion or scatter.

The probability distribution function (pdf), which was the derivative of the joint probability failure function $F(S)$, illustrated the statistical dispersion (Figure 1). Figure 1 exhibited low dispersion or scatter for a high shape parameter combination ($\alpha_1 = 60$ and $\alpha_2 = 60$) and exhibited high dispersion or scatter for a low shape parameter combination ($\alpha_1 = 5$ and $\alpha_2 = 5$). Figure 1 was based on the applied stress ratio at the zero (0) degree

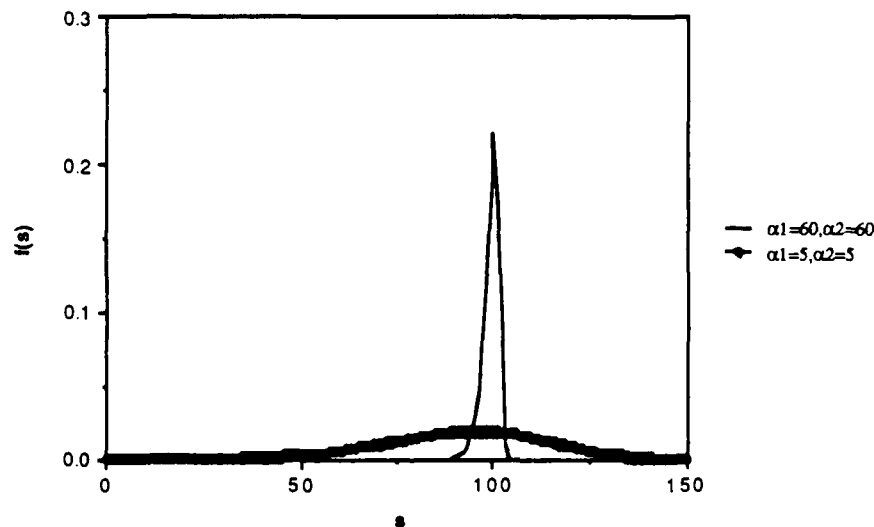


Figure 1

PDF—NORMALIZED $\theta=0$

radial loading path in the normalized stress domain (i.e., the uniaxial case along the longitudinal or fiber direction).

At the applied stress ratios for the normalized stress domain zero (0) and ninety (90) degree radial loading paths, the joint probability function was equivalent to the Weibull distribution function in the uniaxial longitudinal and transverse directions respectively. As a result, the joint probability function was characterized by a unimodal (one statistical mode) distribution (Figure 2).

Figures 3 and 4 exhibited the combined stress state probability distribution functions (pdf) at the applied stress ratio for the normalized stress domain forty-five (45) degree radial loading path. For the high-low shape parameter combination ($\alpha_1 = 60$ and $\alpha_2 = 5$) and the low-high shape parameter combination ($\alpha_1 = 5$ and $\alpha_2 = 60$), the joint probability function was characterized by a bimodal (two statistical modes interacting) distribution.

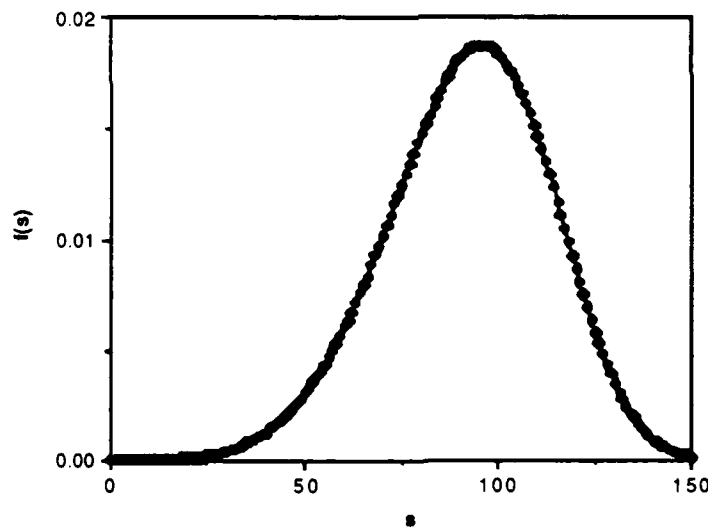


Figure 2

PDF—NORMALIZED $\alpha_1=5, \alpha_2=5, \theta=0$

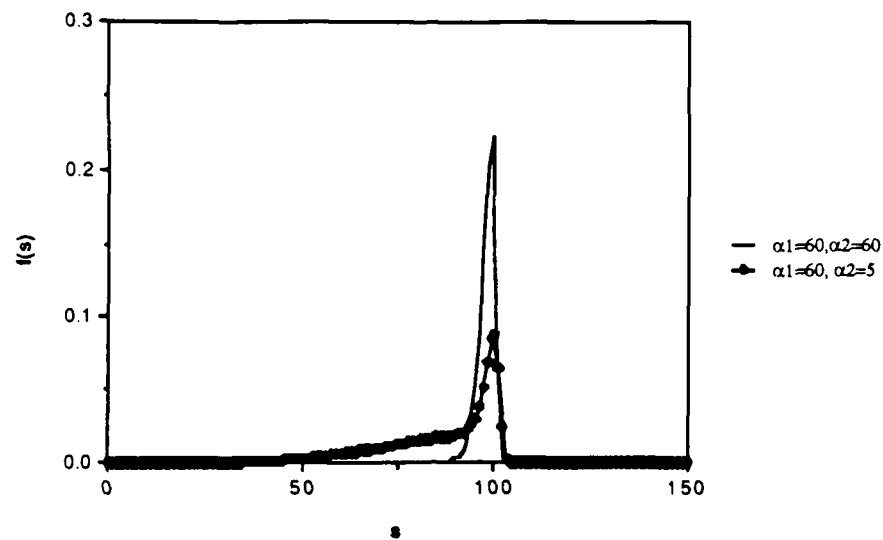


Figure 3

PDF—NORMALIZED $\theta=45$

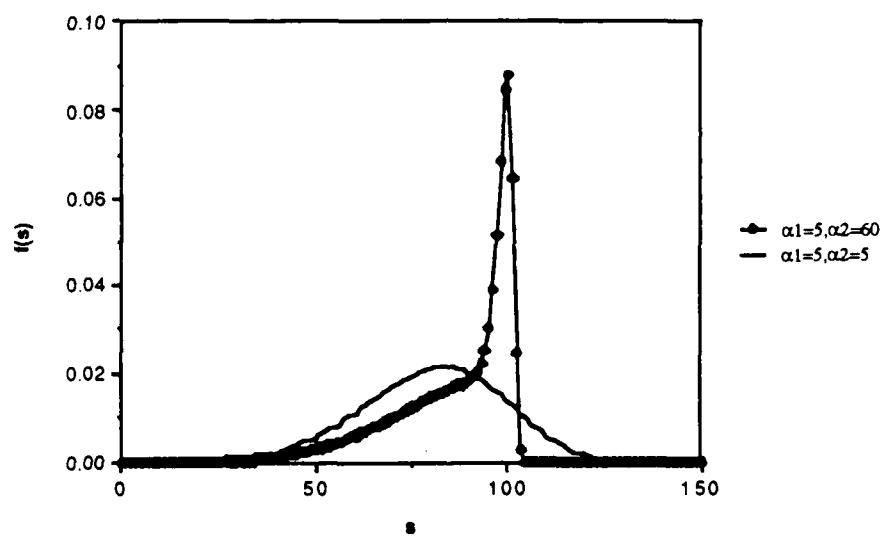


Figure 4

PDF—NORMALIZED $\theta=45$

For the high ($\alpha_1 = 60$ and $\alpha_2 = 60$) and low ($\alpha_1 = 5$ and $\alpha_2 = 5$) shape parameter combinations, the joint probability function was not distinguishable from the unimodal distribution.

It was observed that the joint probability function changed from an unimodal to a bimodal distribution as the combined applied stress ratio changed. The bimodal distribution with the two statistical modes interacting was of special interest to the probabilistic independent and mechanistic independent case.

B . THEORETICAL MATHEMATICAL MODEL

In order to investigate the shape of the failure surface, a numerical simulation was used to study the theoretical mathematical model at seventeen (17) applied stress ratios for a particular sample size and a particular high and/or low combination of the joint probability function shape parameters (α_1 and α_2). The numerical simulation explored the following aspects of the theoretical mathematical model for a particular sample size, applied stress ratio, and shape parameter combination in the stress domain:

- (1) the joint probability reliability and failure functions
- (2) the relative frequency strength
- (3) the mean strength
- (4) the percentile strength
- (5) the mean and percentile strength contours.

For the theoretical mathematical model, the failure envelope or failure surface was defined as:

- (1) The mean strength contour which was normalized by the uniaxial scale parameters (β_1 and β_2).
- (2) The mean strength contour which was normalized by the mean strengths at the uniaxial longitudinal and transverse radial loading paths.

- (3) The percentile strength contours which were normalized by the uniaxial scale parameters (β_1 and β_2).

The mean strength and/or percentile strength contours were expressed at the seventeen (17) applied stress ratios for a large sample size, and as a function of a particular shape parameter (α_1 and α_2) combination.

C. BIAXIAL L/T NUMERICAL SIMULATION

In the stress domain the numerical simulation was used to study seventeen (17) different applied stress ratios for a particular sample size and a particular high and/or low combination of the joint probability function shape parameters (α_1 and α_2). For the numerical simulation a sample size (N) of 199 was selected and was based the concept of Expected Rank, where the fractional probability was defined as $N/(N+1)$. The most important aspects of the numerical simulation for a particular sample size, applied stress ratio and shape parameter combination in the stress domain were:

- (1) the intrinsic strength space
- (2) the realized strength space
- (3) the relative frequency strength space
- (4) the joint probability strength space
- (5) the mean realized strength at different biaxial stress ratios and the mean realized strength contour.

For the numerical simulation the failure envelope or failure surface was defined as:

- (1) the mean realized strength contour of the seventeen (17) applied stress ratios for 199 samples and a particular shape parameter combination and was normalized by the uniaxial scale parameters (β_1 and β_2).
- (2) the mean realized strength contour of the seventeen (17) applied stress ratios for 199 samples and a particular shape parameter combination and was normalized by the mean strength at uniaxial longitudinal and transverse radial loading paths.

IV. RESULTS

A. BIAXIAL L/T NUMERICAL SIMULATION

Figures 5, 6, 7, and 8 illustrated the numerical simulation for an applied stress ratio equivalent to the forty-five (45) degree radial loading path in the normalized stress domain. In order to develop an optimal experimental method for determination of the failure criteria for a given composite material, one must infer the intrinsic strength space (ISS) from the realized strength space (RSS). Figure 5 characterizes the intrinsic strength space (ISS) in the stress domain for the probabilistic independent and mechanistic independent case and a particular combination of the joint probability function scale (β_1 and β_2) and shape (α_1 and α_2) parameters.

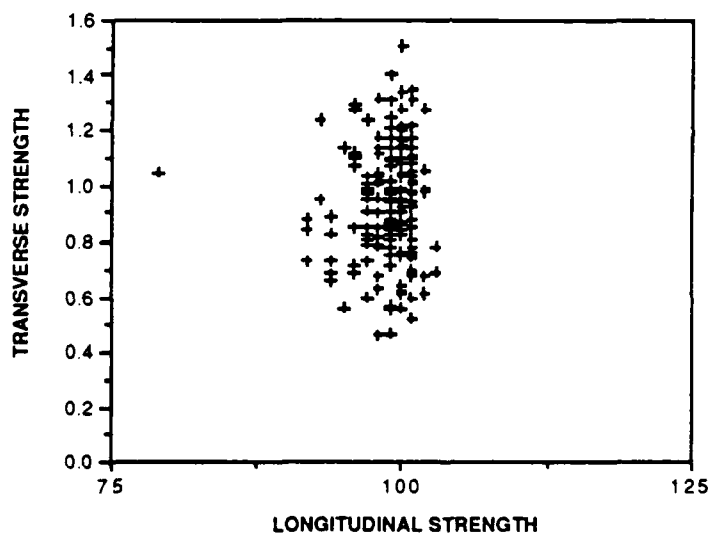


Figure 5

Intrinsic Strength Space $\theta=45$

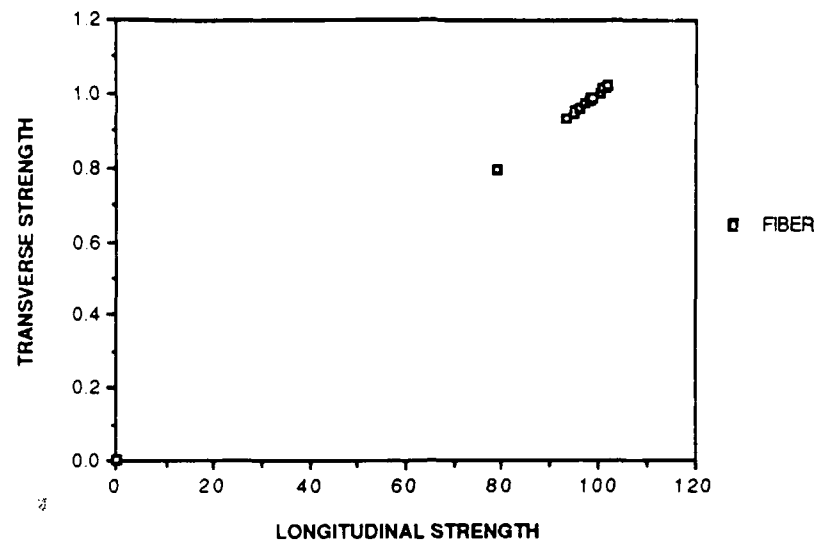


Figure 6

Realized Strength Space $\theta=45$

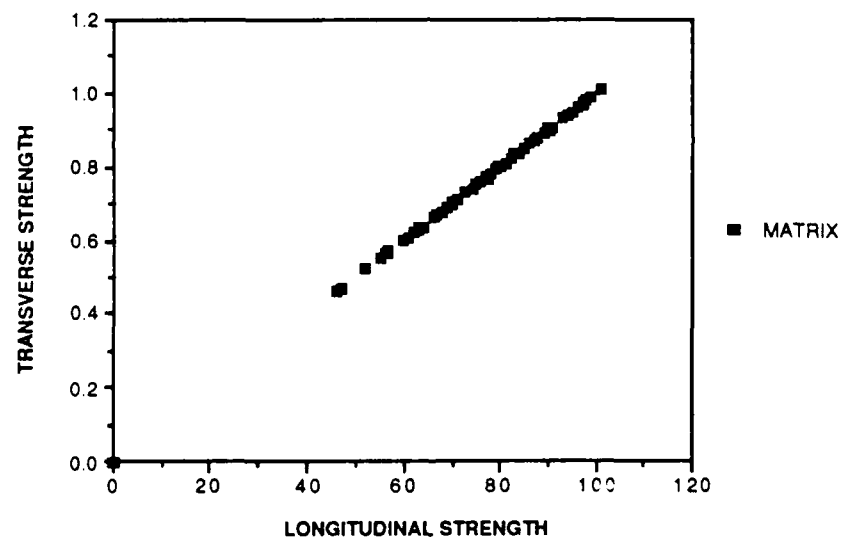


Figure 7

Realized Strength Space $\theta=45$

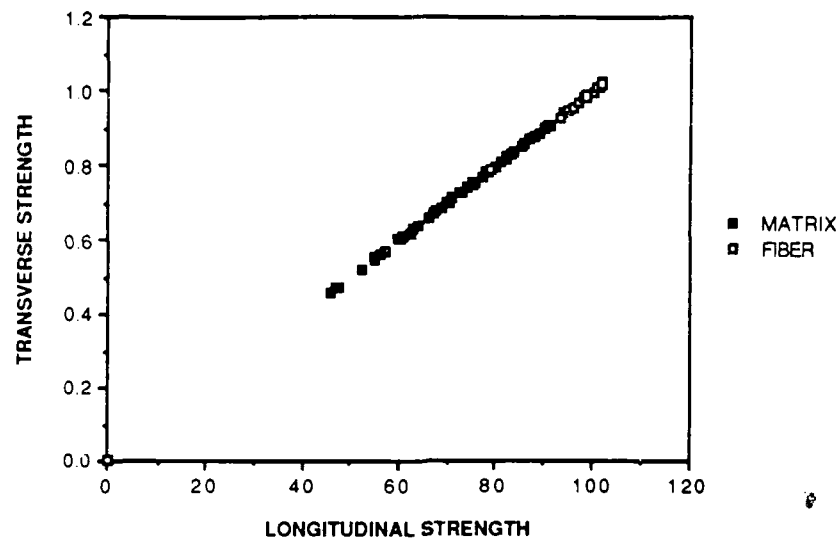


Figure 8

Realized Strength Space $\theta=45$

Figures 6, 7, and 8 depicted the realized strength space (RSS) for an applied stress ratio equivalent to the forty-five (45) degree radial loading path in the normalized stress domain and a particular combination of the joint probability function scale (β_1 and β_2) and shape (α_1 and α_2) parameters. Figure 6 described the RSS for the composite samples associated with fiber failure. Figure 7 described the RSS for the composite samples associated with matrix failure. Figure 8 described the RSS for the composite samples which failed by fiber and/or matrix. The failure modes were observed by the intermixing of the opened and closed points.

Figure 9 was based on the initial conditions and exhibited the realized strength space in the stress domain for five (5) different normalized applied stress ratios at the ten (10), thirty (30), forty-five (45), sixty (60), and eighty (80) degree radial loading paths and for the particular combination of the joint probability function scale (β_1 and β_2) and shape (α_1

and α_2) parameters. This RSS exhibited which composite samples failed by fiber and/or by matrix for various applied stress ratios.

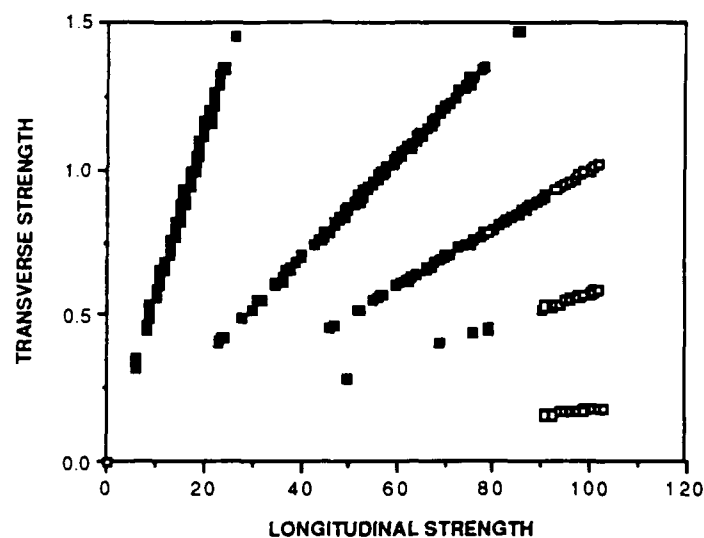


Figure 9

Realized Strength Space $\theta=10, 30, 45, 60, 80$

Figures 10 and 11 were based on the numerical simulation initial conditions for an applied stress ratio equivalent to the forty-five (45) degree radial loading path in the normalized stress domain and a particular combination of the joint probability function scale (β_1 and β_2) and shape (α_1 and α_2) parameters. Figure 10 described the biaxial relative frequency strength space in the stress domain and Figure 11 described the biaxial joint probability strength space in the Weibull probability space. The biaxial relative frequency strength space exhibited the fraction of the sample distribution which failed by fiber and/or matrix. A unimodal Weibull cumulative distribution function appears as a linear function in the Weibull probability space. Of particular interest to this study was that the joint probability strength space was not linear. This was due to the bimodal condition where

two statistical modes were interacting. For reliability, the lower tail of a particular sample distribution was of major importance in the development of any failure criterion.

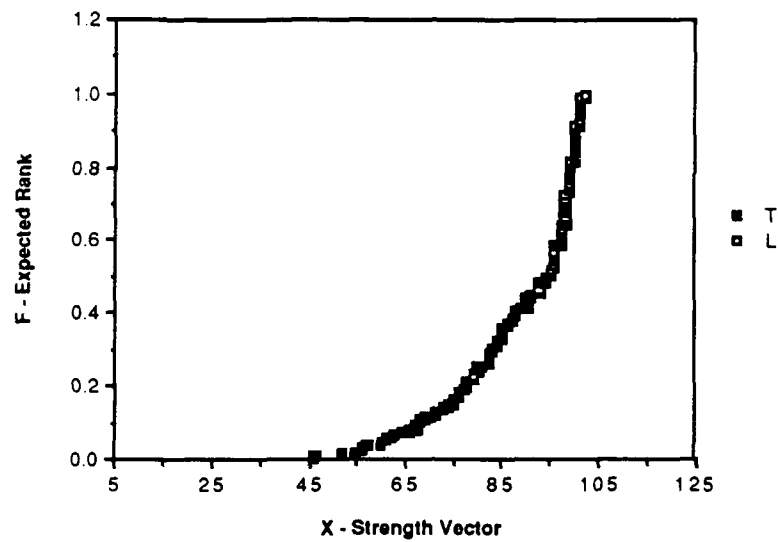


Figure 10

Relative Frequency Strength Space $\theta=45$

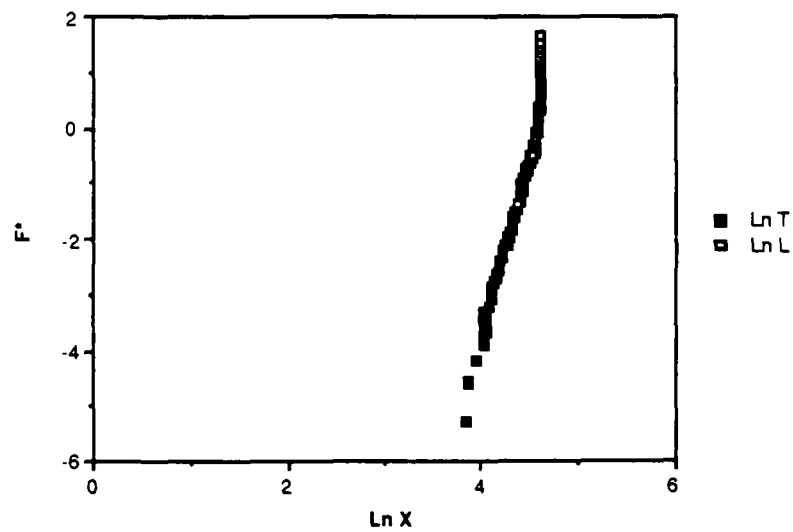


Figure 11

Joint Probability Strength Space $\theta=45$

Figures 12 and 13 described a mean realized strength contour in the stress domain which was based on the numerical simulation of the seventeen (17) discrete applied stress ratios and the joint probability scale (β_1 and β_2) and shape (α_1 and α_2) parameters. Figure 12 was normalized by the uniaxial scale parameters (β_1 and β_2) and Figure 13 was normalized by the uniaxial mean strength at the applied stress ratios equivalent to the zero (0) and ninety (90) degree radial loading paths in the normalized stress domain.

For the biaxial L/T numerical simulation, the mean realized strength contour defined the failure envelope or failure surface in the stress domain. Biaxial stress states interior to the domain bounded by the failure envelope or failure surface was the safe region. Biaxial stress states exterior to the domain bounded by the failure envelope or failure surface was the unsafe region.

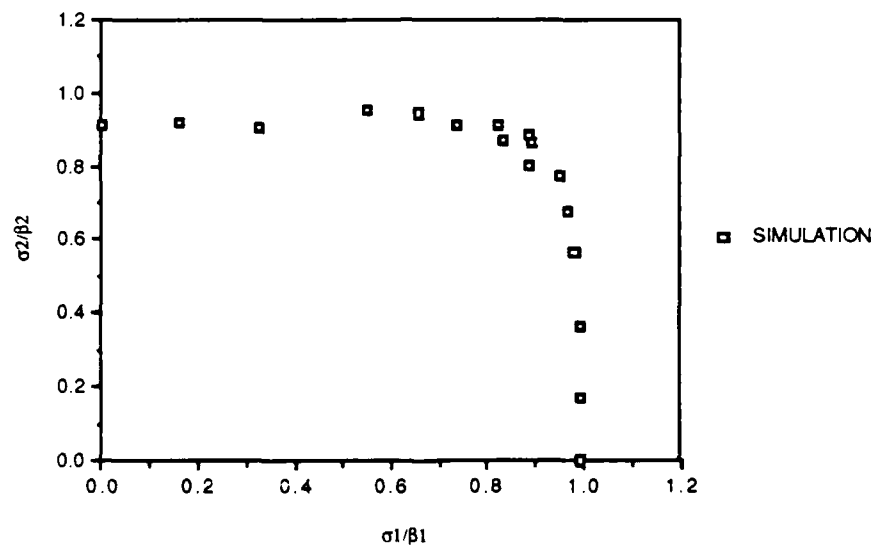


Figure 12

Failure Envelope or Failure Surface

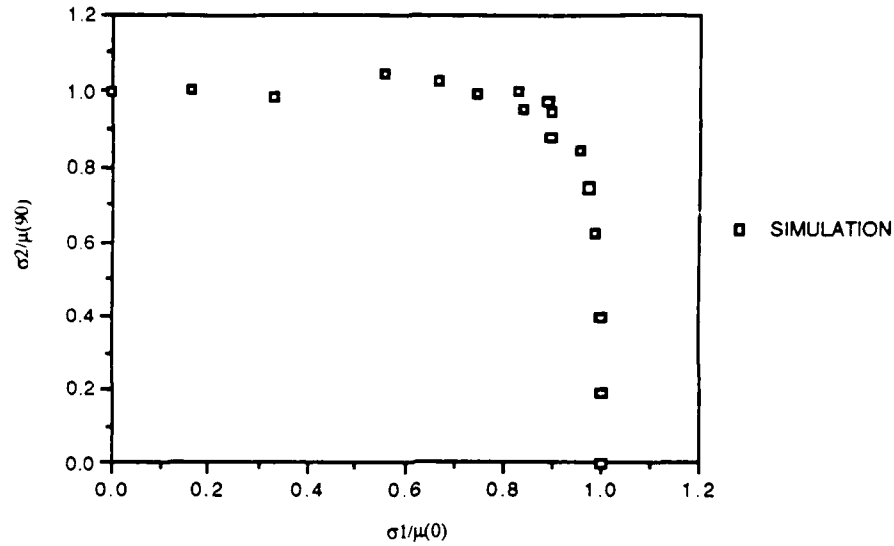


Figure 13

Failure Envelope or Failure Surface

B. ANALYTICAL EVALUATION OF MODEL

Figures 14 and 15 described the theoretical mathematical model failure functions in the stress domain for five (5) applied stress ratios and were based on the particular combination of the joint probability scale (β_1 and β_2) and shape (α_1 and α_2) parameters. The five (5) normalized applied stress ratios were based on the zero (0), thirty-nine (39), forty-five (45), fifty-one (51), and ninety (90) degree radial loading paths. The trends for increasing the transformed theta from the normalized zero (0) degree radial loading path in the longitudinal or fiber direction to the normalized ninety (90) degree radial loading path in the transverse or matrix direction were that the failure function curves shifted to the left.

Figures 16 and 17 described the joint probability failure function and reliability function in the stress domain for the applied stress ratio based on the normalized forty-five (45) degree radial loading path. By analyzing the longitudinal or fiber and the transverse or matrix components of the reliability and failure functions, one observed, in this particular

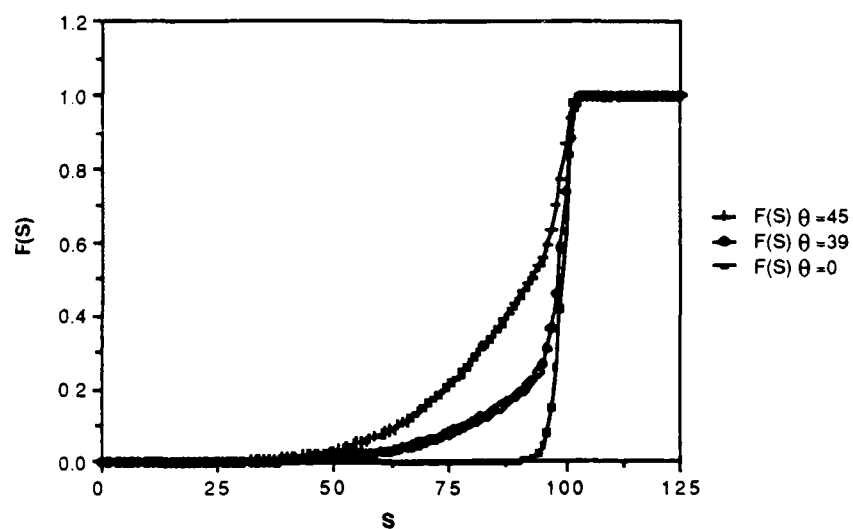


Figure 14

Failure Function $\alpha_1=60, \alpha_2=5$

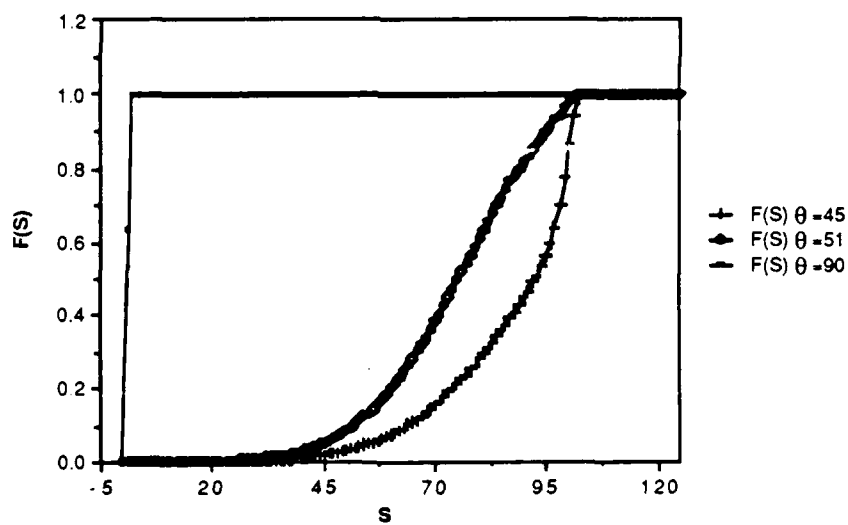


Figure 15

Failure Function $\alpha_1=60, \alpha_2=5$

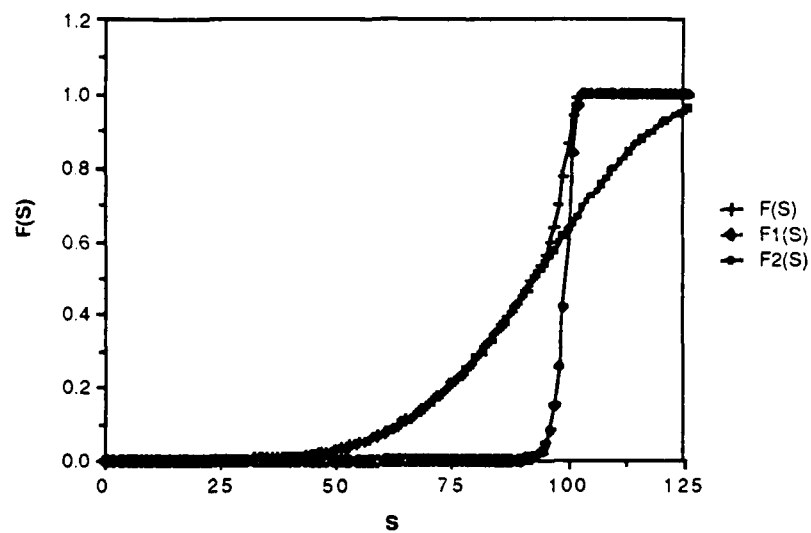


Figure 16

Failure Function $\alpha_1=60, \alpha_2=5, \theta=45$

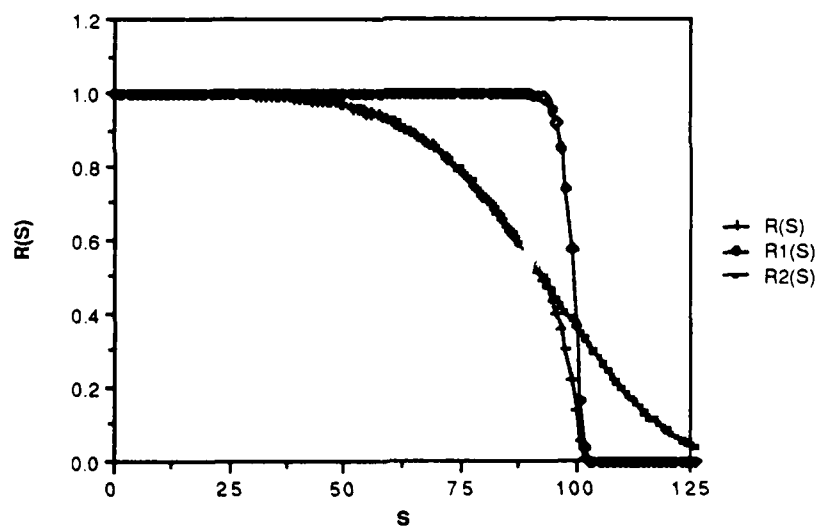


Figure 17

Reliability Function $\alpha_1=60, \alpha_2=5, \theta=45$

case, that there exists a transition area or crossover area, where the two joint probability functions were a function of both components in the fiber and matrix directions. As a result, both the reliability and failure functions were characterized by a bimodal distribution where two statistical modes were interacting.

Figure 18 exhibited the failure function at the applied stress ratio based on the normalized forty-five (45) degree radial loading path for the theoretical model with the numerical simulation biaxial relative frequency strength space superimposed. Figure 19 exhibited the failure function and the longitudinal or fiber and transverse or matrix components of the failure function with the numerical simulation biaxial relative frequency strength space superimposed. Figure 19 exhibited the fiber and matrix transition or crossover area of the sample distribution, which was characterized by the two failure function components interacting.

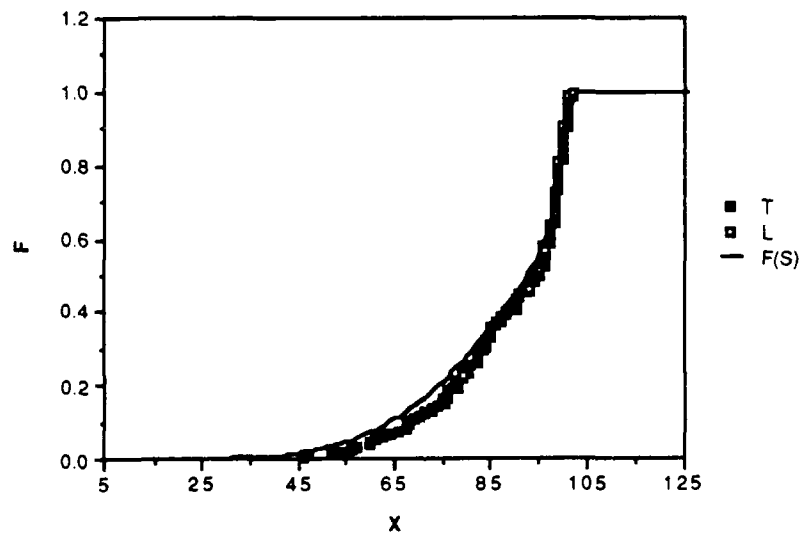


Figure 18

Relative Frequency Strength Space $\theta=45$

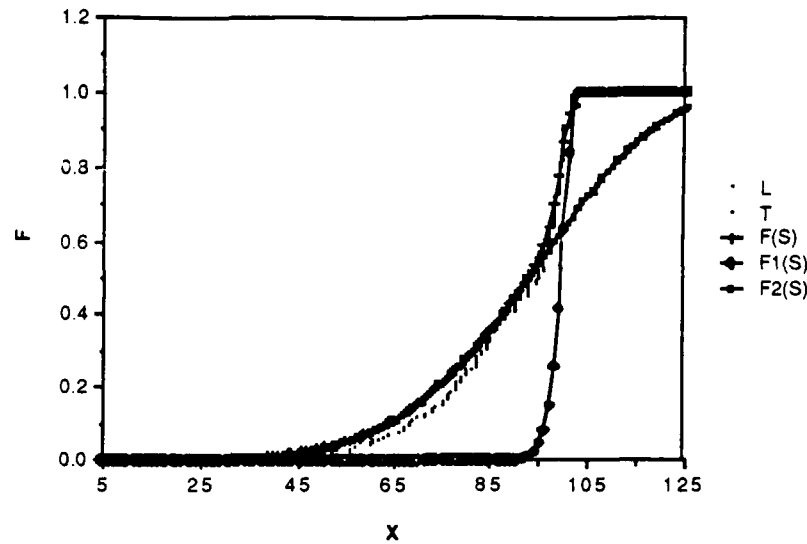


Figure 19

Relative Frequency Strength Space $\theta=45$

Figures 20 and 21 exhibited the analytical mean strength contour evaluated at the seventeen (17) applied stress ratios with the biaxial numerical simulated mean realized strength contour superimposed. Figure 20 was normalized by the uniaxial scale parameters (β_1 and β_2). Figure 21 was normalized by the uniaxial mean strength at the applied stress ratios equivalent to the zero (0) and ninety (90) degree radial loading paths in the normalized stress domain. Either mean strength contour defined the failure envelopes or failure surfaces in the failure domain which was superimposed in the stress domain.

Figures 22 and 23 exhibited the analytical mean strength contour (failure envelope or failure surface) which was normalized by the uniaxial scale parameters (β_1 and β_2) with the percentile strength contours (failure envelope or failure surface) at the ten (10) percentile and the ninety (90) percentile superimposed. In Figure 23 the biaxial numerical simulation mean strength contour was superimposed. From the theoretical model one would

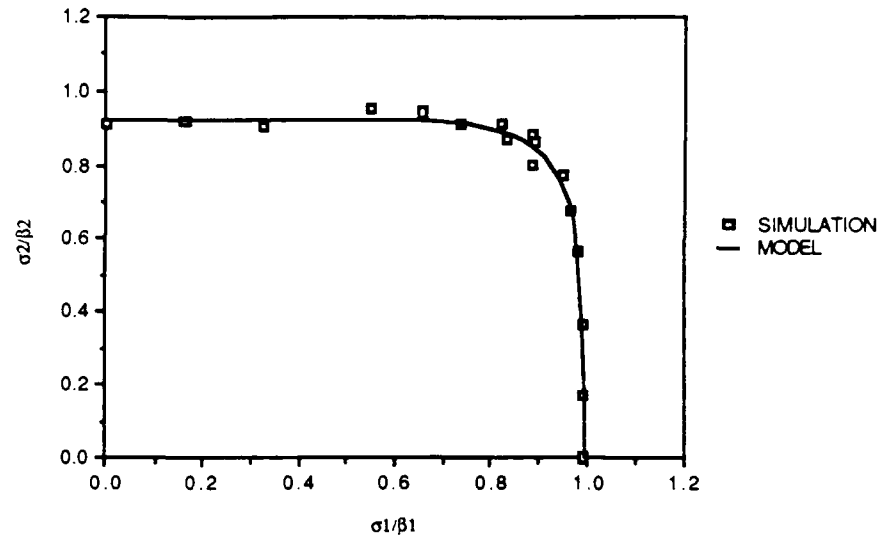


Figure 20

Failure Envelope or Failure Surface

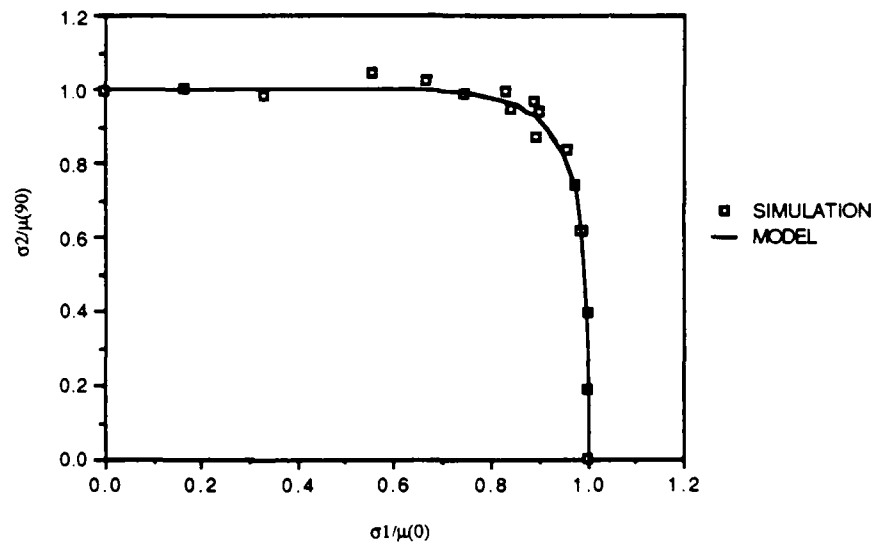


Figure 21

Failure Envelope or Failure Surface

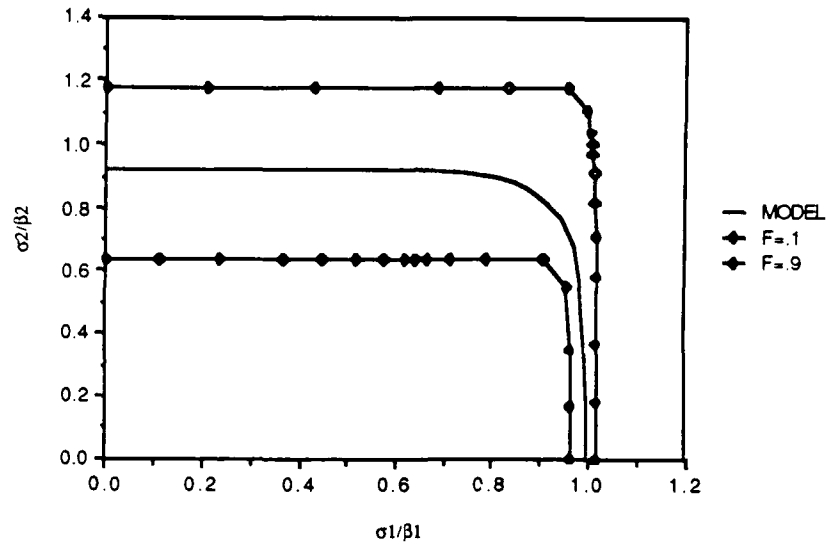


Figure 22

Failure Envelope or Failure Surface

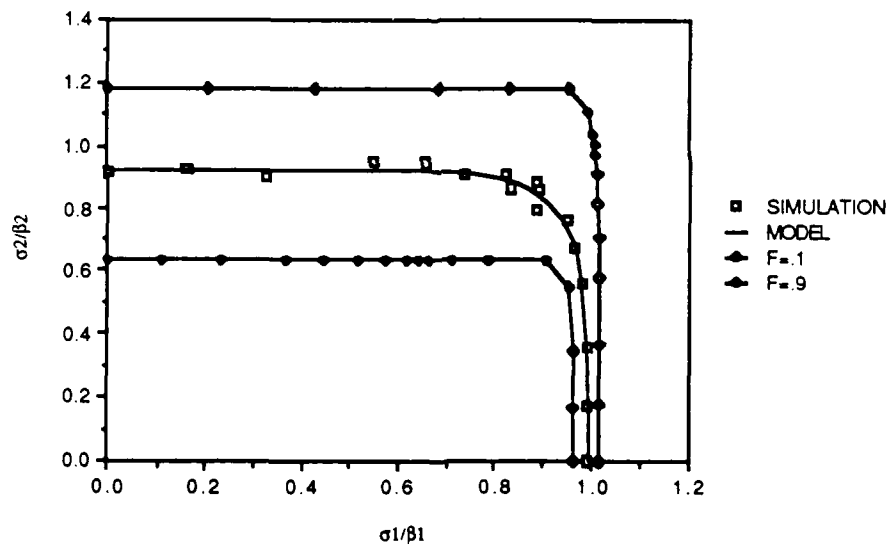


Figure 23

Failure Envelope or Failure Surface

analytically develop percentile contour failure envelopes in order to describe the fraction of the sample distribution which failed (lower bound or worst case).

Figures 24, 25, 26, 27, and 28 were based on the initial conditions and the particular combination of the joint probability scale and shape parameters and exhibited the analytical failure distribution in the stress domain as a function of the changes in the applied stress ratios. The normalized applied stress ratios were based on the fifty-five (55), forty-eight (48), forty-two (42), thirty-five (35), and thirty (30) degree radial loading paths. The objective was to analyze the unimodal and bimodal distributions of the analytical failure function over a particular applied stress ratio range. At the normalized fifty-five (55) degree radial loading path, the theoretical failure function was not distinguishable from a unimodal distribution. This would indicate that practically all composite failures were caused by matrix failure. At the normalized thirty (30) degree radial loading path the theoretical failure function also approached a unimodal distribution. This would indicate that

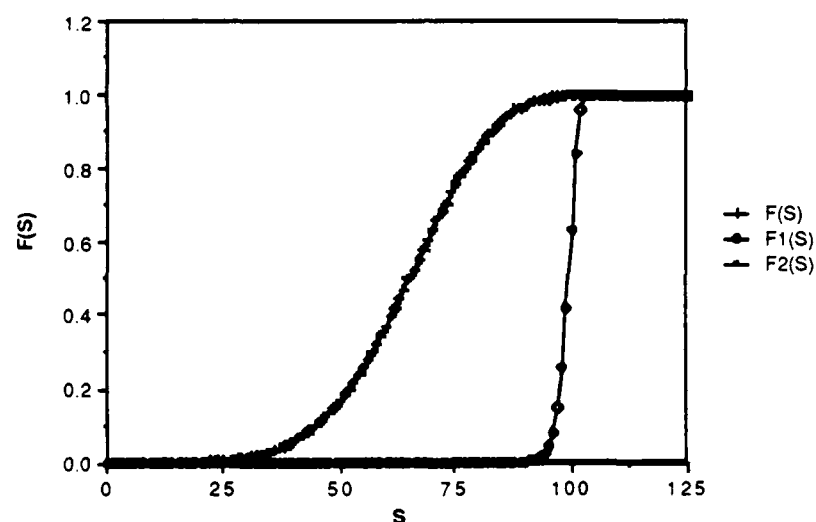


Figure 24

Failure Function $\alpha_1=60$, $\alpha_2=5$, $\theta=55$

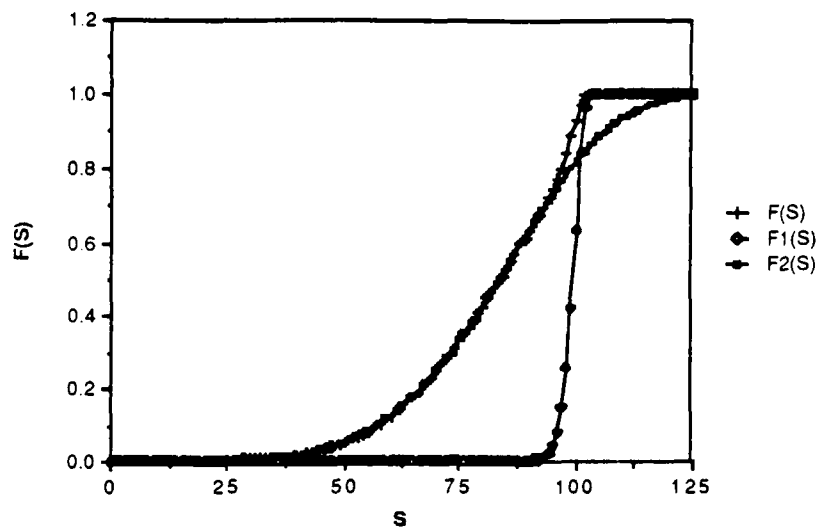


Figure 25

Failure Function $\alpha_1=60, \alpha_2=5, \theta=48$

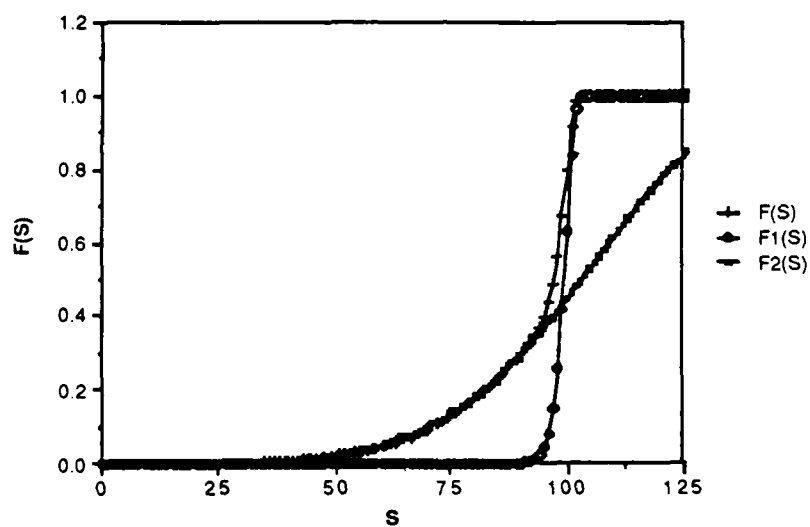


Figure 26

Failure Function $\alpha_1=60, \alpha_2=5, \theta=42$

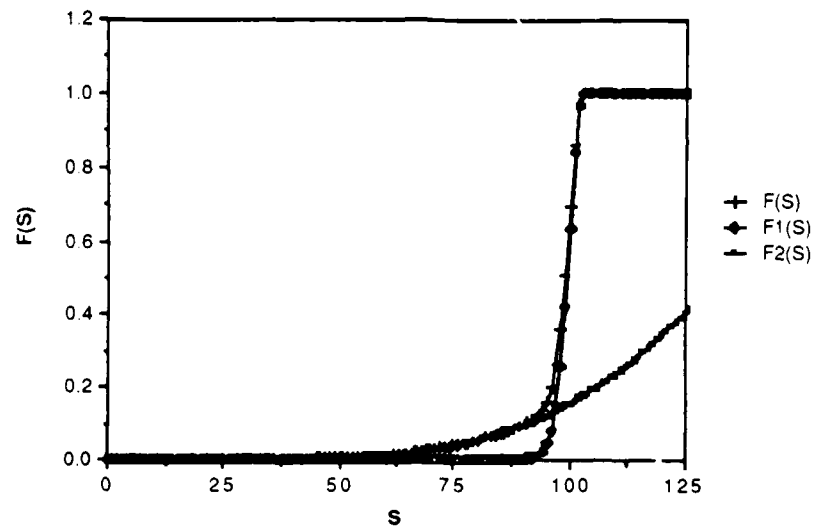


Figure 27

Failure Function $\alpha_1=60, \alpha_2=5, \theta=35$

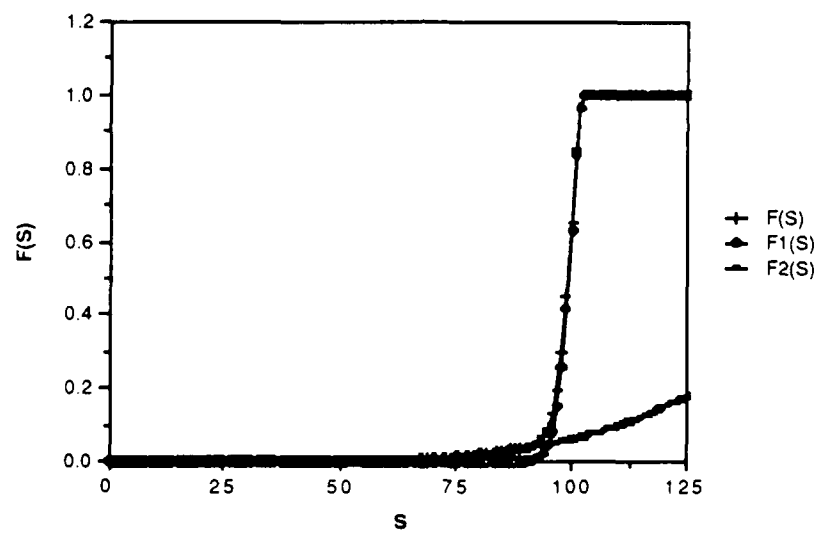


Figure 28

Failure Function $\alpha_1=60, \alpha_2=5, \theta=30$

practically all composite failures were caused by fiber failure. The failure functions associated with the normalized applied stress ratios at the forty-eight (48), forty-two (42), and thirty-five (35) radial loading paths were characterized as a bimodal distribution by the failure function component transition or crossover region. This would indicate that the composite failures were caused by both fiber failures and matrix failures.

From this demonstration one could conclude that there existed a specific applied stress ratio range where the failure function as well as the reliability function would exhibit a bimodal distribution and a specific applied stress ratio range where both functions would exhibit an unimodal distribution. Of primary interest was the bimodal distributions where two statistical modes were interacting.

Figures 29, 30, and 31 were based on the initial conditions and an applied stress ratio normalized at the forty-five (45) degree radial loading path and exhibited the theoretical failure function in the stress domain as a function of the changes in the joint probability shape parameters (α_1 and α_2). Figures 29 and 31 exhibited that the failure functions associated with the high-high ($\alpha_1 = 60$ and $\alpha_2 = 60$) and low-low ($\alpha_1 = 5$ and $\alpha_2 = 5$) joint probability shape parameter combinations were not distinguishable from the unimodal distribution. Figure 30 exhibited that the failure function associated with the medium-low ($\alpha_1 = 20$ and $\alpha_2 = 5$) joint probability shape parameter combination was characterized by a bimodal distribution.

From this demonstration one could conclude that the bimodal distribution was attributed to the degree of dispersion or scatter as exhibited by the various combinations of the joint probability shape parameters. A high-high joint probability shape parameter combination would exhibit a very narrow applied stress ratio range for the bimodal distribution. A low-low joint probability shape parameter combination would exhibit a large applied stress ratio range for the bimodal distribution. As a result, a high-high joint probability

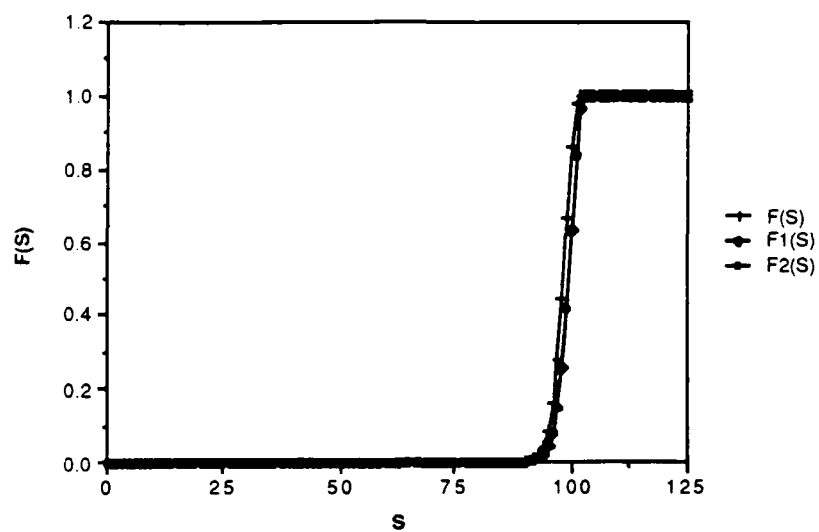


Figure 29

Failure Function $\alpha_1=60$, $\alpha_2=60$, $\theta=45$

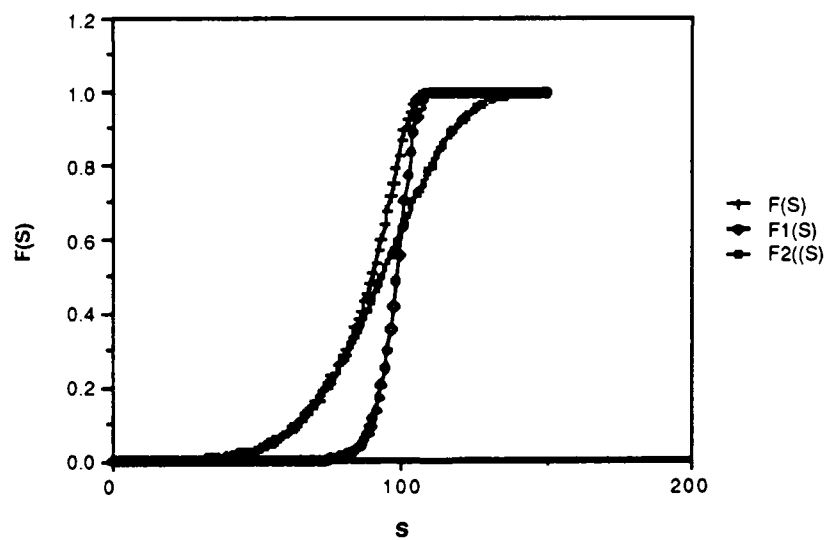


Figure 30

Failure Function $\alpha_1=20$, $\alpha_2=5$, $\theta=45$

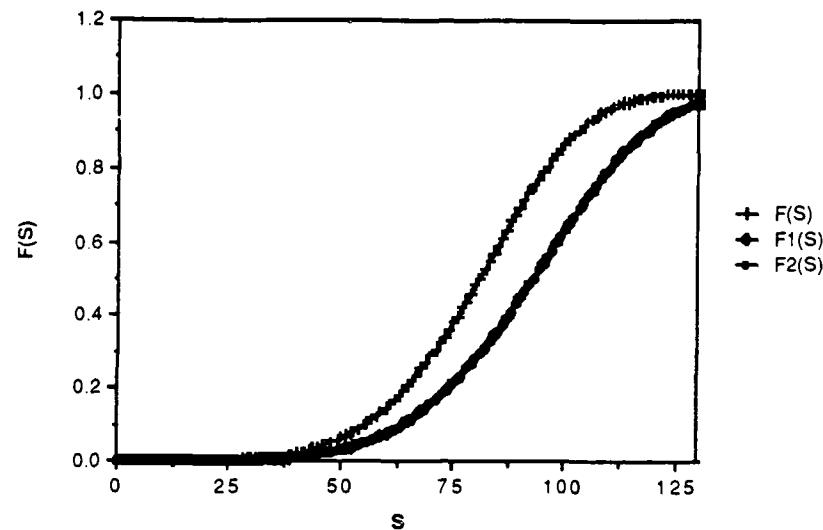


Figure 31

Failure Function $\alpha_1=5, \alpha_2=5, \theta=45$

shape parameter combination was recommended for little or no dispersion (scatter) in the stress domain.

Figures 32 and 33 exhibited the analytical mean strength contours which were based on the initial conditions, the seventeen (17) applied stress ratios, and changes in the joint probability shape parameters (α_1 and α_2). The results indicated that the failure envelope or failure surface area decreased in size with decreases in the joint probability shape parameter combinations. In addition, the results indicated that the failure envelopes or failure surfaces changed from an independent appearance at the high-high joint probability shape parameter combination ($\alpha_1 = 60$ and $\alpha_2 = 60$) to a dependent appearance for the remaining joint probability shape parameter combinations.

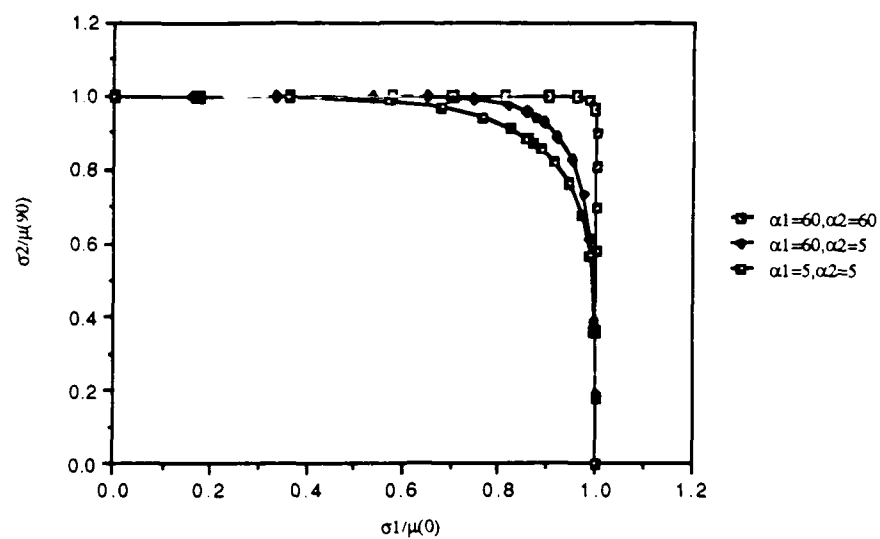


Figure 32

Failure Envelope or Failure Surface

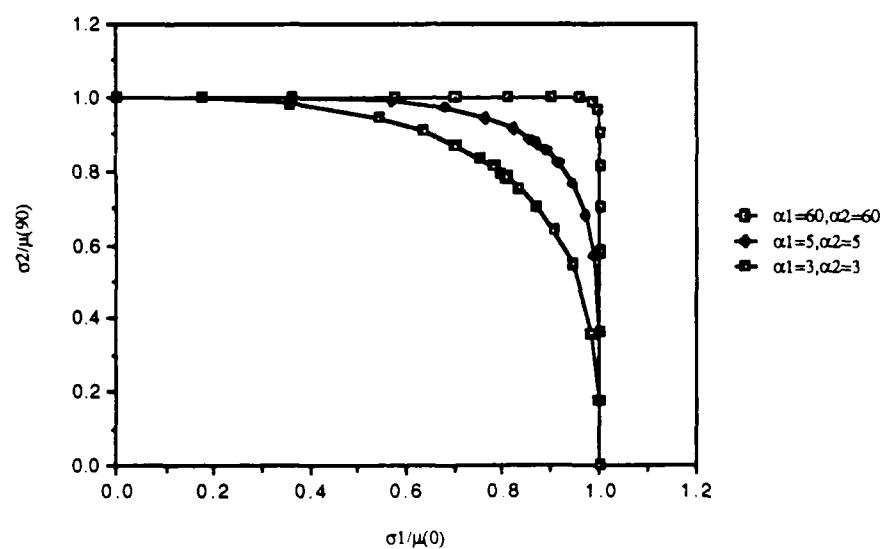


Figure 33

Failure Envelope or Failure Surface

Based on a Weibull weakest link (L) formulation [Ref. 14]:

$$\beta_2 = \beta_1 \left(\frac{L_2}{L_1} \right)^{-1/\alpha}$$

where

$$\begin{aligned} \beta_2 < \beta_1 & \quad \text{if } \alpha > 1 \text{ and} \\ & \quad \text{for } L_2 > L_1 \end{aligned}$$

The objective was to demonstrate the role of the shape parameter (α) on the size and mean strength of a particular structure. If the size of a particular structure increased (L_2) with the shape parameter (α) fixed, then the mean strength would decrease based on $\beta_2 < \beta_1$. In addition, if the shape parameter (α) decreased (increased dispersion) with the size fixed, then the mean strength of a particular structure would decrease based on $\beta_2 < \beta_1$.

From this demonstration one could conclude that a high-high shape parameter combination exhibited a large failure envelope or failure surface (safe region) with little or no dispersion (scatter) and a very narrow range where the two failure statistical modes interacted. In other words, the size and shape of the failure envelope or failure surface was largely dependent on the joint probability shape parameters (α_1 and α_2).

V. CONCLUSIONS AND RECOMMENDATIONS

For the probabilistic and mechanistic independent case, the failure envelope or failure surface as presented by a mean strength contour (failure criterion) in this particular study gave the phenomenological appearance of mechanistic dependency. This result would give the erroneous inference that the intrinsic strengths were coupled and dependent, and the failure mechanisms were interacting. Whereas, this study demonstrated that the size and shape of the phenomenological failure envelope or failure surface were dependent on the strength variability of the uniaxial shape parameter (α_1 and α_2) combinations.

This study covered the two dimensional probabilistic independent and mechanistic independent case. As for recommendations, further analysis in three dimensions (including the case where the shear stress is non-zero) is required as well as an extension to the other three cases:

1. probabilistic dependent and mechanistic independent case.
2. probabilistic independent and mechanistic dependent case.
3. probabilistic dependent and mechanistic dependent case.

The objective is to infer the intrinsic strength space from the realized strength space via a numerical simulation of an analytical model for each of the four cases. Numerical simulation would identify the cause (or modes) of failure whether it was by fiber failure, or by matrix failure, or by shear failure. The failure mechanisms cannot be readily identified with the analytical model. Such understanding would form definitive recommendations for composite material development, such as identifying the benefits associated with improving the fiber or matrix or the interface in order to achieve the desired reliability under combined stress state conditions. Identification of the failure modes by numerical simulation would also aid the definition of experimental detection techniques for quality assurance.

APPENDIX A

THEORETICAL MATHEMATICAL MODEL

The theoretical model was derived for a stress domain and was expressed as a function of a strength vector, an applied stress ratio (radial loading path), and the joint probability function shape (α) and scale (β) parameters. The applied stress ratio in the normalized domain (normalized by β_1 and β_2) was equivalent to the transformed theta (θ), and was defined as (Figure 34):

$$\theta_1 = \tan^{-1} [(\sigma_2/\sigma_1) * (\beta_1/\beta_2)]$$

where:

(1) $\sigma_2/\sigma_1 = \tan(\theta_1) * (\beta_2/\beta_1)$ in the normalized domain.

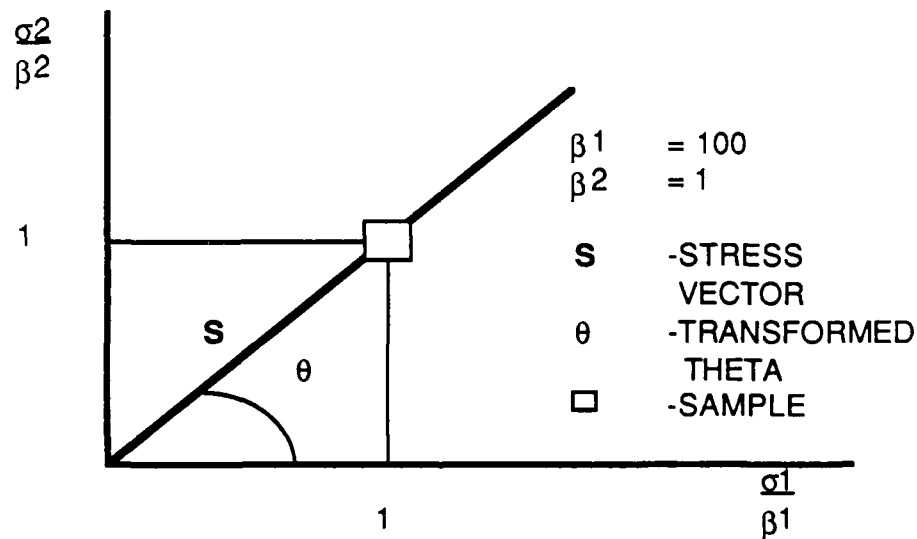


Figure 34

Applied Stress Ratio in Normalized Domain

The applied stress ratio in the stress domain was equivalent to the physical theta (θ) and was defined as:

$$\theta = \tan^{-1} (\sigma_2/\sigma_1).$$

The transformed theta was used in determining the physical theta in the stress domain. Therefore, the applied stress ratio in the stress domain for this study was defined as (Figure 35):

$$\theta = \tan^{-1} [\tan (\theta_1) * (\beta_2/\beta_1)]$$

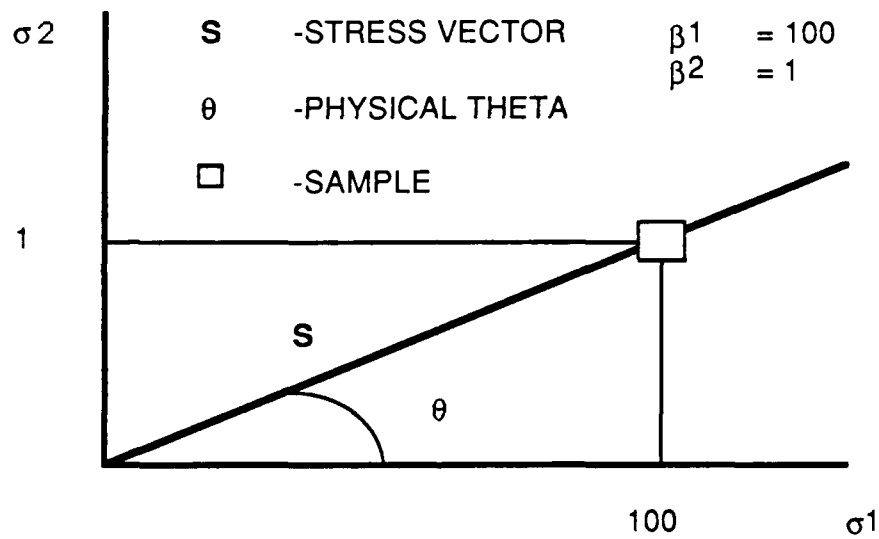


Figure 35

Applied Stress Ratio in Physical Domain

In the stress domain the stress component in the longitudinal or fiber direction was defined by a strength vector (S) as:

$$\sigma_1 = (|S|) * \cos (\theta).$$

The stress component in the transverse or matrix direction was defined by a strength vector (S) as:

$$\sigma_2 = (|S|) * \sin (\theta).$$

Based on joint probability [$R(|S|) = R_1(|S|) * R_2(|S|)$], the theoretical model reliability function in the stress domain was expressed as:

$$R(|S|) = \exp [-(|S| * \cos (\theta) / \beta_1)^{\alpha_1}] * \exp [-(|S| * \sin (\theta) / \beta_2)^{\alpha_2}].$$

The theoretical model failure function in the stress domain was defined as:

$$F(|S|) = 1 - R(|S|)$$

$$F(|S|) = 1 - [\exp [-(|S| * \cos (\theta) / \beta_1)^{\alpha_1}] * \exp [-(|S| * \sin (\theta) / \beta_2)^{\alpha_2}]].$$

where:

- (1) $R(|S|)$ was the joint probability reliability function.
- (2) $F(|S|)$ was the joint probability failure function.
- (3) $(|S|) * \cos (\theta)$ was the strength component in the longitudinal or fiber direction as defined by the strength vector (S).
- (4) $(|S|) * \sin (\theta)$ was the strength component in the transverse or matrix direction as defined by the strength vector (S).
- (5) α_1 and β_1 were the joint probability shape (A1 or alfa1) and scale (B1 or beta1) parameters respectively in longitudinal or fiber direction.
- (6) α_2 and β_2 were the joint probability shape (A2 or alfa2) and scale (B2 or beta2) parameters respectively in transverse or matrix direction.

The theoretical model defined the fail envelope or failure surface by a mean strength distribution or contour and a percentile strength distribution or contour for the seventeen

(17) applied stress ratios, a particular sample size, and a particular combination of the joint probability shape parameters (α_1 and α_2).

The theoretical mean failure surface, as defined by a mean strength distribution or contour, was derived from the concept of Expected Value [Ref. 15]:

$$\mu = \int xf(x) dx$$

$$\mu = \int [1-F(|S|)] ds$$

where:

- (1) $1 - F(|S|)$ is the theoretical reliability function $[R(|S|)]$.

A Gauss Quadrature method for the integration of the Expected Value mean $[\mu = \int [1-F(|S|)] ds]$ was used to find the mean strength distribution or contour (Appendix D). The percentile failure surface, as defined by the percentile strength distribution or contour, was an iterative process of the failure function $F(|S|)$ (Appendix G).

APPENDIX B

BIAXIAL L/T NUMERICAL SIMULATION

The numerical simulation of a theoretical model was equivalent to actual experimental testing. The biaxial L/T numerical simulation was a function of intrinsic strengths, an applied stress ratio (radial loading path), and the joint probability function shape (α) and scale (β) parameters. The applied stress ratio in the normalized domain (normalized by β_1 and β_2) was equivalent to the transformed theta (θ) and was defined as (Figure 36):

$$\theta = \tan^{-1} (T/L * \beta_1/\beta_2)$$

where:

- (1) T is the transverse stress in the matrix direction.
- (2) L is the longitudinal stress in the fiber direction.

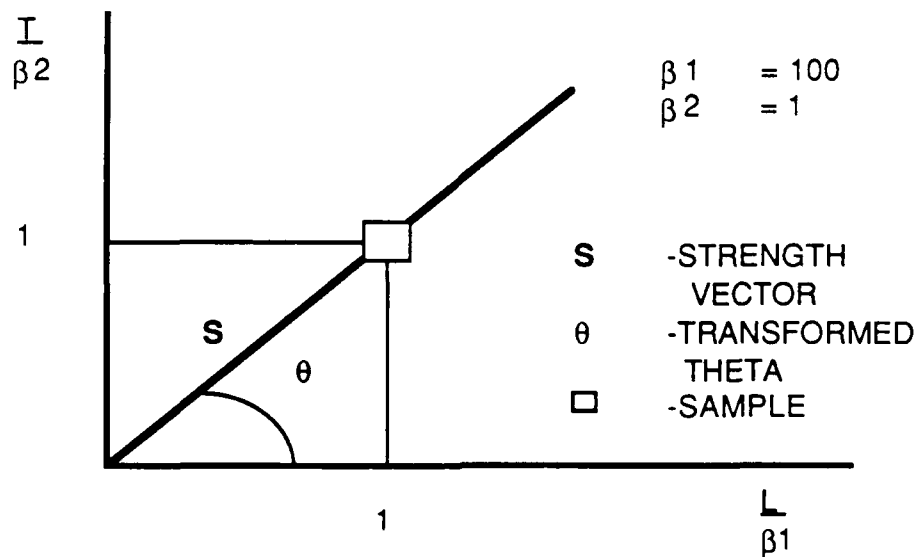


Figure 36

Applied Stress Ratio in Normalized Domain

The transformed theta was used to determine the biaxial L/T (longitudinal/transverse) applied stress ratio in the stress domain. Therefore, the applied stress ratio in the stress domain for this study was defined as (Figure 37):

$$\text{BIAXIAL } L/T = (\beta_1/\beta_2) / \tan(\theta).$$

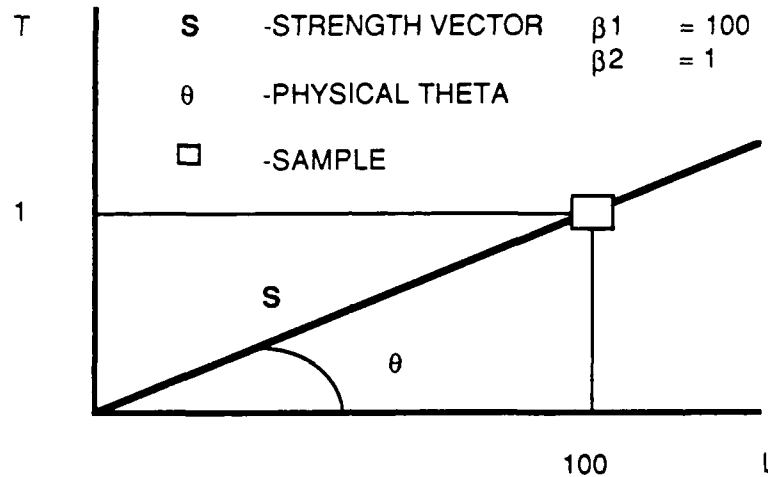


Figure 37

Applied Stress Ratio in Physical Domain

The biaxial numerical simulation was based on the joint probability reliability function $[R(X) = R_1(X_1) * R_2(X_2)]$. The numerical simulation reliability function and failure function in the stress domain were defined respectively as:

$$R(X) = \exp [-(X_1/\beta_1)^{\alpha_1} + (X_2/\beta_2)^{\alpha_2}]$$

$$F(X) = 1 - R(X) = 1 - \exp [-(X_1/\beta_1)^{\alpha_1} + (X_2/\beta_2)^{\alpha_2}]$$

where:

- (1) $R(X)$ was the reliability function and was equivalent to the probability of success associated with the random variables X_1 and X_2 .

- (2) $F(X)$ was the failure function and was equivalent to the probability of failure associated with the random variables X_1 and X_2 .
- (3) X_1 was the random intrinsic strength in the longitudinal or fiber direction.
- (4) X_2 was the random intrinsic strength in the transverse or matrix direction.
- (5) α_1 and β_1 were the joint probability shape (A_1 or α_1) and scale (B_1 or β_1) parameters respectively in the longitudinal or fiber direction.
- (6) α_2 and β_2 were the joint probability shape (A_2 or α_2) and scale (B_2 or β_2) parameters respectively in the transverse or matrix direction.

For the numerical simulation X_1/X_2 was the intrinsic strength ratio and biaxial L/T was the applied stress ratio in the stress domain. Under a combined stress state, the following strength and stress conditions in the realized strength space were evaluated by the numerical simulation:

- (1) If $X_1/X_2 < \text{biaxial } L/T$, the composite failed by fiber (Figure 38).
- (2) If $X_1/X_2 > \text{biaxial } L/T$, the composite failed by matrix (Figure 39).
- (3) If $X_1/X_2 = \text{biaxial } L/T$, the composite failed by both fiber and matrix. [Ref. 16]

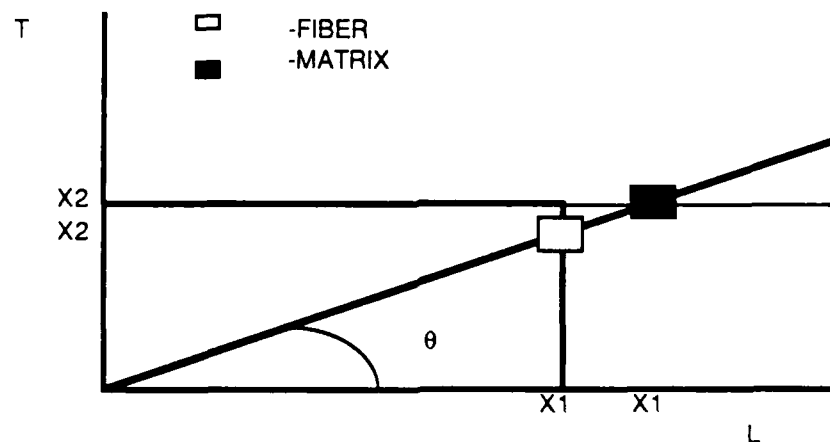


Figure 38

Composite Fails by Fiber

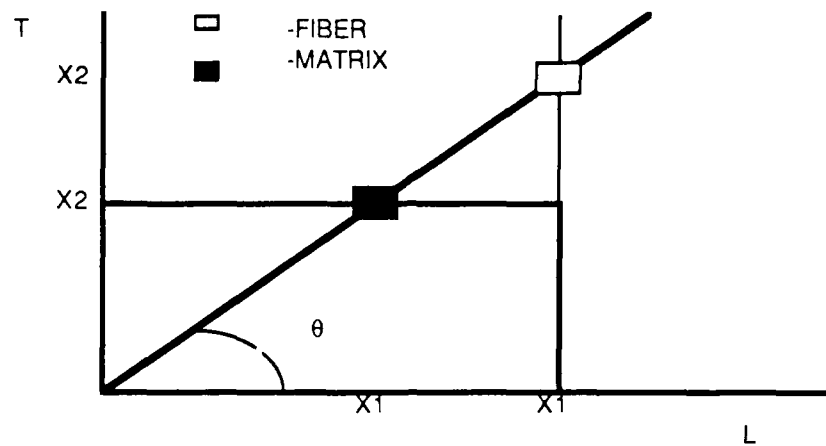


Figure 39

Composite Fails by Matrix

Joint probability for this study was defined as the intrinsic strength which was activated by the stress (σ_1) in the longitudinal or fiber direction was independent of the intrinsic strength which was activated by the stress (σ_2) in the transverse or matrix direction. The strengths were uncoupled and the failure mechanisms were not interacting. An example follows (Figure 40):

Take a composite that has high strength in matrix ($X2'$) and low strength in fiber ($X1'$), the composite sample failed by fiber. Take a composite that has medium strength in matrix ($X2''$) and medium strength in fiber ($X1''$), the composite sample in this case failed by fiber. Take a composite that has low strength in matrix ($X2'''$) and high strength in fiber ($X1'''$), the composite sample failed by matrix. [Ref. 17]

For the numerical simulation the absolute intrinsic strengths for each sample defined the intrinsic (not observable) strength space (ISS) via a spatial point in the biaxial stress domain. The combined strength-stress ratio comparison defined the realized (observable) strength space (RSS) via a strength vector in the biaxial stress domain.

The biaxial numerical simulation failure envelope or failure surface in the stress domain was defined by a mean strength distribution or contour, where the mean strength was defined as the sum of the realized strength vectors divided by the number of samples

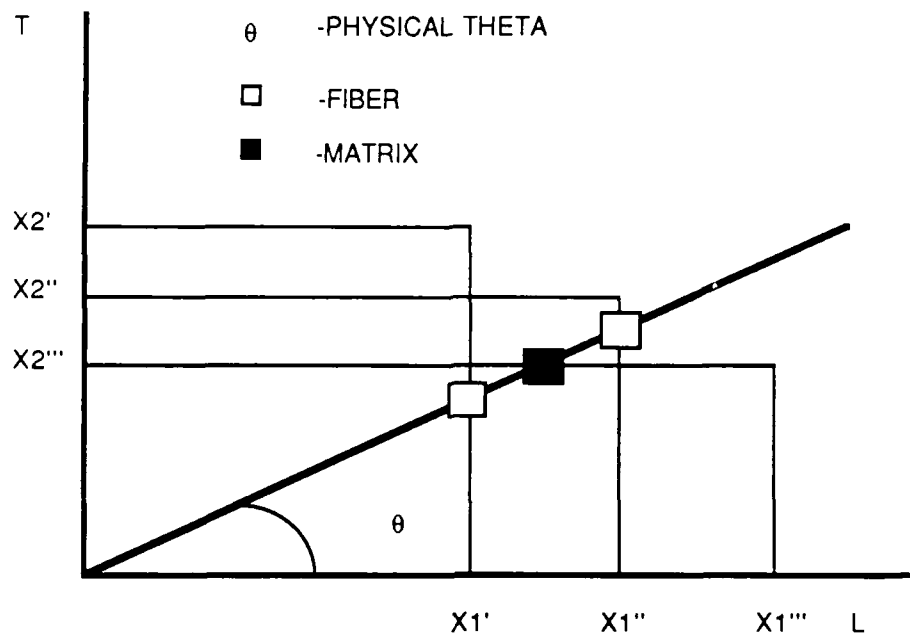


Figure 40

Joint Probability (Independent) Realized Strength Space

for each of the seventeen (17) applied stress ratios, and was a function of a particular sample size and a particular combination of the joint probability function shape parameters (α_1 and α_2).

Appendix C exhibited two biaxial L/T numerical simulation worksheets. One was to describe the formulation of the numerical simulation. The second was to provide an example of the numerical simulation.

APPENDIX C

NUMERICAL SIMULATION FORMULATION

The most important aspects of the biaxial L/T numerical simulation [Ref. 18] for a particular sample size, applied stress ratio and the joint probability scale (β_1 and β_2) and shape (α_1 and α_2) parameters in the stress domain were:

- (1) the intrinsic strength space
- (2) the realized strength space
- (3) the relative frequency strength space
- (4) the joint probability strength space
- (5) the mean realized strength and the mean realized strength distribution

The first worksheet described the formulation of the numerical simulation. The second worksheet provided an example numerical simulation that was based on a sample size of 19, an applied stress ratio normalized for the forty-five (45) degree radial loading path, and the joint probability shape ($\alpha_1 = 60$ and $\alpha_2 = 5$) and scale ($\beta_1 = 100$ and $\beta_2 = 1$) parameters. The worksheets were based on Microsoft Excel software.

A		B		C		D	
1	alfa1	60		physical theta		biaxial L/T	
2	beta1	100				radian	
3	alfa2	5		transformed theta		Theta	
4	beta2	1					
5							
6	alfa and beta						
7	are shape and scale					columns D and E define the intrinsic strength	
8	parameters respectively					space (ISS)	
9							
10							
11			column B defines	column C defines			
12			relative intrinsic	relative intrinsic			
13			strength in the	strength in the		column D defines	
14			longitudinal or fiber	transverse or matrix		absolute intrinsic strength in the longitudinal or	
15			direction	direction		fiber direction	
16							
17							
18						Fiber	
19			random	random		strength	
20			number	number		X1	
21	1	=RAND() + 0.000001		=RAND() + 0.000001		=EXP((LN(-LN(1-B21)) + alfa1 * LN(beta1)) / alfa1)	
22	=A21 + 1	=RAND() + 0.000001		=RAND() + 0.000001		=EXP((LN(-LN(1-B22)) + alfa1 * LN(beta1)) / alfa1)	
23	=A22 + 1	=RAND() + 0.000001		=RAND() + 0.000001		=EXP((LN(-LN(1-B23)) + alfa1 * LN(beta1)) / alfa1)	
24	=A23 + 1	=RAND() + 0.000001		=RAND() + 0.000001		=EXP((LN(-LN(1-B24)) + alfa1 * LN(beta1)) / alfa1)	
25	=A24 + 1	=RAND() + 0.000001		=RAND() + 0.000001		=EXP((LN(-LN(1-B25)) + alfa1 * LN(beta1)) / alfa1)	
26	=A25 + 1	=RAND() + 0.000001		=RAND() + 0.000001		=EXP((LN(-LN(1-B26)) + alfa1 * LN(beta1)) / alfa1)	
27	=A26 + 1	=RAND() + 0.000001		=RAND() + 0.000001		=EXP((LN(-LN(1-B27)) + alfa1 * LN(beta1)) / alfa1)	
28	=A27 + 1	=RAND() + 0.000001		=RAND() + 0.000001		=EXP((LN(-LN(1-B28)) + alfa1 * LN(beta1)) / alfa1)	
29	=A28 + 1	=RAND() + 0.000001		=RAND() + 0.000001		=EXP((LN(-LN(1-B29)) + alfa1 * LN(beta1)) / alfa1)	
30	=A29 + 1	=RAND() + 0.000001		=RAND() + 0.000001		=EXP((LN(-LN(1-B30)) + alfa1 * LN(beta1)) / alfa1)	
31	=A30 + 1	=RAND() + 0.000001		=RAND() + 0.000001		=EXP((LN(-LN(1-B31)) + alfa1 * LN(beta1)) / alfa1)	
32	=A31 + 1	=RAND() + 0.000001		=RAND() + 0.000001		=EXP((LN(-LN(1-B32)) + alfa1 * LN(beta1)) / alfa1)	
33	=A32 + 1	=RAND() + 0.000001		=RAND() + 0.000001		=EXP((LN(-LN(1-B33)) + alfa1 * LN(beta1)) / alfa1)	
34	=A33 + 1	=RAND() + 0.000001		=RAND() + 0.000001		=EXP((LN(-LN(1-B34)) + alfa1 * LN(beta1)) / alfa1)	
35	=A34 + 1	=RAND() + 0.000001		=RAND() + 0.000001		=EXP((LN(-LN(1-B35)) + alfa1 * LN(beta1)) / alfa1)	
36	=A35 + 1	=RAND() + 0.000001		=RAND() + 0.000001		=EXP((LN(-LN(1-B36)) + alfa1 * LN(beta1)) / alfa1)	
37	=A36 + 1	=RAND() + 0.000001		=RAND() + 0.000001		=EXP((LN(-LN(1-B37)) + alfa1 * LN(beta1)) / alfa1)	
38	=A37 + 1	=RAND() + 0.000001		=RAND() + 0.000001		=EXP((LN(-LN(1-B38)) + alfa1 * LN(beta1)) / alfa1)	
39	=A38 + 1	=RAND() + 0.000001		=RAND() + 0.000001		=EXP((LN(-LN(1-B39)) + alfa1 * LN(beta1)) / alfa1)	
40							
41							

	E	F	G	H
1	$=(\beta_1/\beta_2)/\tan(\text{radian})$			
2	$=(3.1415926535278/180) \cdot \theta$			
3	45			
4				
5				
6				
7			columns G to J define the realized stress space (RSS)	columns G to J are the comparison of intrinsic strength ratio to biaxial L/T applied stress ratio
8				
9				
10				
11		column F		
12		defines		
13	column E defines		column G defines	column H defines
14	absolute intrinsic strength in the transverse or	intrinsic strength	fiber strength associated with	matrix strength associated with
15	matrix direction	ratio	fiber failure	fiber failure
16				
17				
18	Matrix		Fiber	Fiber
19	strength		fails	fails
20	X2	X1 / X2	L	T
21	$=\exp((\ln(-\ln(1-C_{21}))+\alpha_1\alpha_2^2\ln(\beta_2))/\alpha_1\alpha_2)$	$=D_{21}/E_{21}$	$=\text{IF}(F_{21}<\text{biaxial}, D_{21}, 0.001)$	$=\text{IF}(F_{21}<\text{biaxial}, D_{21}/\text{biaxial}, 0.001)$
22	$=\exp((\ln(-\ln(1-C_{22}))+\alpha_1\alpha_2^2\ln(\beta_2))/\alpha_1\alpha_2)$	$=D_{22}/E_{22}$	$=\text{IF}(F_{22}<\text{biaxial}, D_{22}, 0.001)$	$=\text{IF}(F_{22}<\text{biaxial}, D_{22}/\text{biaxial}, 0.001)$
23	$=\exp((\ln(-\ln(1-C_{23}))+\alpha_1\alpha_2^2\ln(\beta_2))/\alpha_1\alpha_2)$	$=D_{23}/E_{23}$	$=\text{IF}(F_{23}<\text{biaxial}, D_{23}, 0.001)$	$=\text{IF}(F_{23}<\text{biaxial}, D_{23}/\text{biaxial}, 0.001)$
24	$=\exp((\ln(-\ln(1-C_{24}))+\alpha_1\alpha_2^2\ln(\beta_2))/\alpha_1\alpha_2)$	$=D_{24}/E_{24}$	$=\text{IF}(F_{24}<\text{biaxial}, D_{24}, 0.001)$	$=\text{IF}(F_{24}<\text{biaxial}, D_{24}/\text{biaxial}, 0.001)$
25	$=\exp((\ln(-\ln(1-C_{25}))+\alpha_1\alpha_2^2\ln(\beta_2))/\alpha_1\alpha_2)$	$=D_{25}/E_{25}$	$=\text{IF}(F_{25}<\text{biaxial}, D_{25}, 0.001)$	$=\text{IF}(F_{25}<\text{biaxial}, D_{25}/\text{biaxial}, 0.001)$
26	$=\exp((\ln(-\ln(1-C_{26}))+\alpha_1\alpha_2^2\ln(\beta_2))/\alpha_1\alpha_2)$	$=D_{26}/E_{26}$	$=\text{IF}(F_{26}<\text{biaxial}, D_{26}, 0.001)$	$=\text{IF}(F_{26}<\text{biaxial}, D_{26}/\text{biaxial}, 0.001)$
27	$=\exp((\ln(-\ln(1-C_{27}))+\alpha_1\alpha_2^2\ln(\beta_2))/\alpha_1\alpha_2)$	$=D_{27}/E_{27}$	$=\text{IF}(F_{27}<\text{biaxial}, D_{27}, 0.001)$	$=\text{IF}(F_{27}<\text{biaxial}, D_{27}/\text{biaxial}, 0.001)$
28	$=\exp((\ln(-\ln(1-C_{28}))+\alpha_1\alpha_2^2\ln(\beta_2))/\alpha_1\alpha_2)$	$=D_{28}/E_{28}$	$=\text{IF}(F_{28}<\text{biaxial}, D_{28}, 0.001)$	$=\text{IF}(F_{28}<\text{biaxial}, D_{28}/\text{biaxial}, 0.001)$
29	$=\exp((\ln(-\ln(1-C_{29}))+\alpha_1\alpha_2^2\ln(\beta_2))/\alpha_1\alpha_2)$	$=D_{29}/E_{29}$	$=\text{IF}(F_{29}<\text{biaxial}, D_{29}, 0.001)$	$=\text{IF}(F_{29}<\text{biaxial}, D_{29}/\text{biaxial}, 0.001)$
30	$=\exp((\ln(-\ln(1-C_{30}))+\alpha_1\alpha_2^2\ln(\beta_2))/\alpha_1\alpha_2)$	$=D_{30}/E_{30}$	$=\text{IF}(F_{30}<\text{biaxial}, D_{30}, 0.001)$	$=\text{IF}(F_{30}<\text{biaxial}, D_{30}/\text{biaxial}, 0.001)$
31	$=\exp((\ln(-\ln(1-C_{31}))+\alpha_1\alpha_2^2\ln(\beta_2))/\alpha_1\alpha_2)$	$=D_{31}/E_{31}$	$=\text{IF}(F_{31}<\text{biaxial}, D_{31}, 0.001)$	$=\text{IF}(F_{31}<\text{biaxial}, D_{31}/\text{biaxial}, 0.001)$
32	$=\exp((\ln(-\ln(1-C_{32}))+\alpha_1\alpha_2^2\ln(\beta_2))/\alpha_1\alpha_2)$	$=D_{32}/E_{32}$	$=\text{IF}(F_{32}<\text{biaxial}, D_{32}, 0.001)$	$=\text{IF}(F_{32}<\text{biaxial}, D_{32}/\text{biaxial}, 0.001)$
33	$=\exp((\ln(-\ln(1-C_{33}))+\alpha_1\alpha_2^2\ln(\beta_2))/\alpha_1\alpha_2)$	$=D_{33}/E_{33}$	$=\text{IF}(F_{33}<\text{biaxial}, D_{33}, 0.001)$	$=\text{IF}(F_{33}<\text{biaxial}, D_{33}/\text{biaxial}, 0.001)$
34	$=\exp((\ln(-\ln(1-C_{34}))+\alpha_1\alpha_2^2\ln(\beta_2))/\alpha_1\alpha_2)$	$=D_{34}/E_{34}$	$=\text{IF}(F_{34}<\text{biaxial}, D_{34}, 0.001)$	$=\text{IF}(F_{34}<\text{biaxial}, D_{34}/\text{biaxial}, 0.001)$
35	$=\exp((\ln(-\ln(1-C_{35}))+\alpha_1\alpha_2^2\ln(\beta_2))/\alpha_1\alpha_2)$	$=D_{35}/E_{35}$	$=\text{IF}(F_{35}<\text{biaxial}, D_{35}, 0.001)$	$=\text{IF}(F_{35}<\text{biaxial}, D_{35}/\text{biaxial}, 0.001)$
36	$=\exp((\ln(-\ln(1-C_{36}))+\alpha_1\alpha_2^2\ln(\beta_2))/\alpha_1\alpha_2)$	$=D_{36}/E_{36}$	$=\text{IF}(F_{36}<\text{biaxial}, D_{36}, 0.001)$	$=\text{IF}(F_{36}<\text{biaxial}, D_{36}/\text{biaxial}, 0.001)$
37	$=\exp((\ln(-\ln(1-C_{37}))+\alpha_1\alpha_2^2\ln(\beta_2))/\alpha_1\alpha_2)$	$=D_{37}/E_{37}$	$=\text{IF}(F_{37}<\text{biaxial}, D_{37}, 0.001)$	$=\text{IF}(F_{37}<\text{biaxial}, D_{37}/\text{biaxial}, 0.001)$
38	$=\exp((\ln(-\ln(1-C_{38}))+\alpha_1\alpha_2^2\ln(\beta_2))/\alpha_1\alpha_2)$	$=D_{38}/E_{38}$	$=\text{IF}(F_{38}<\text{biaxial}, D_{38}, 0.001)$	$=\text{IF}(F_{38}<\text{biaxial}, D_{38}/\text{biaxial}, 0.001)$
39	$=\exp((\ln(-\ln(1-C_{39}))+\alpha_1\alpha_2^2\ln(\beta_2))/\alpha_1\alpha_2)$	$=D_{39}/E_{39}$	$=\text{IF}(F_{39}<\text{biaxial}, D_{39}, 0.001)$	$=\text{IF}(F_{39}<\text{biaxial}, D_{39}/\text{biaxial}, 0.001)$
40				
41				

I		J		K		L	
1				No. of tests	N		
2				calculated	alfa		
3				calculated	beta		
4							
5				numerical simulation	MEAN		
6							
7							
8							
9							
10							
11							
12							
13	column I defines	column J defines					
14	fiber strength associated with	matrix strength associated with					
15	matrix failure	matrix failure					
16							
17							
18	Matrix	Matrix		Fibr fail	Mtrx fail		
19	fails	fails		vector	vector		
20	L	T		L	T		
21	=IF(F21>biaxial, biaxial*E21, 0.001)	=IF(F21>biaxial, E21, 0.001)		=SORT(G21^2+H21^2)	=SORT(I21^2+J21^2)		
22	=IF(F22>biaxial, biaxial*E22, 0.001)	=IF(F22>biaxial, E22, 0.001)		=SORT(G22^2+H22^2)	=SORT(I22^2+J22^2)		
23	=IF(F23>biaxial, biaxial*E23, 0.001)	=IF(F23>biaxial, E23, 0.001)		=SORT(G23^2+H23^2)	=SORT(I23^2+J23^2)		
24	=IF(F24>biaxial, biaxial*E24, 0.001)	=IF(F24>biaxial, E24, 0.001)		=SORT(G24^2+H24^2)	=SORT(I24^2+J24^2)		
25	=IF(F25>biaxial, biaxial*E25, 0.001)	=IF(F25>biaxial, E25, 0.001)		=SORT(G25^2+H25^2)	=SORT(I25^2+J25^2)		
26	=IF(F26>biaxial, biaxial*E26, 0.001)	=IF(F26>biaxial, E26, 0.001)		=SORT(G26^2+H26^2)	=SORT(I26^2+J26^2)		
27	=IF(F27>biaxial, biaxial*E27, 0.001)	=IF(F27>biaxial, E27, 0.001)		=SORT(G27^2+H27^2)	=SORT(I27^2+J27^2)		
28	=IF(F28>biaxial, biaxial*E28, 0.001)	=IF(F28>biaxial, E28, 0.001)		=SORT(G28^2+H28^2)	=SORT(I28^2+J28^2)		
29	=IF(F29>biaxial, biaxial*E29, 0.001)	=IF(F29>biaxial, E29, 0.001)		=SORT(G29^2+H29^2)	=SORT(I29^2+J29^2)		
30	=IF(F30>biaxial, biaxial*E30, 0.001)	=IF(F30>biaxial, E30, 0.001)		=SORT(G30^2+H30^2)	=SORT(I30^2+J30^2)		
31	=IF(F31>biaxial, biaxial*E31, 0.001)	=IF(F31>biaxial, E31, 0.001)		=SORT(G31^2+H31^2)	=SORT(I31^2+J31^2)		
32	=IF(F32>biaxial, biaxial*E32, 0.001)	=IF(F32>biaxial, E32, 0.001)		=SORT(G32^2+H32^2)	=SORT(I32^2+J32^2)		
33	=IF(F33>biaxial, biaxial*E33, 0.001)	=IF(F33>biaxial, E33, 0.001)		=SORT(G33^2+H33^2)	=SORT(I33^2+J33^2)		
34	=IF(F34>biaxial, biaxial*E34, 0.001)	=IF(F34>biaxial, E34, 0.001)		=SORT(G34^2+H34^2)	=SORT(I34^2+J34^2)		
35	=IF(F35>biaxial, biaxial*E35, 0.001)	=IF(F35>biaxial, E35, 0.001)		=SORT(G35^2+H35^2)	=SORT(I35^2+J35^2)		
36	=IF(F36>biaxial, biaxial*E36, 0.001)	=IF(F36>biaxial, E36, 0.001)		=SORT(G36^2+H36^2)	=SORT(I36^2+J36^2)		
37	=IF(F37>biaxial, biaxial*E37, 0.001)	=IF(F37>biaxial, E37, 0.001)		=SORT(G37^2+H37^2)	=SORT(I37^2+J37^2)		
38	=IF(F38>biaxial, biaxial*E38, 0.001)	=IF(F38>biaxial, E38, 0.001)		=SORT(G38^2+H38^2)	=SORT(I38^2+J38^2)		
39	=IF(F39>biaxial, biaxial*E39, 0.001)	=IF(F39>biaxial, E39, 0.001)		=SORT(G39^2+H39^2)	=SORT(I39^2+J39^2)		
40							
41							

	M	N	O	P	Q	R
1	19	(entered data)			1. Set Transformed Theta - applied stress ratio in normalized domain	
2	=Z40	=Z40				
3	=(W40/N)^(1/alfa)	Calc from iteration			2. Calculate via Calculate Now Function	
4					3. Sort NOPORS by ColumnP	
5	=SUM(\$M2:\$M39)/N					
6					4. Copy columns D to E, G to J, and N to U via Scrapbook Function to Cricket Graph	
7						
8						
9						
10						
11					5. columns N to P and U defines the Relative Frequency strength space	
12						
13						
14					6. columns Q to S and T defines the Joint Probability strength space	
15						
16						
17	Realized	Ordered	Ordered	Ordered	Ordered	Ordered
18	Strength	Fibr fail	Mtrx fail	Strength		
19	Vector	vector	vector	Vector		
20	X	L	T	X	In L	In T
21	=K21+L21	=K21	=L21	=M21	=LN(N21)	=LN(O21)
22	=K22+L22	=K22	=L22	=M22	=LN(N22)	=LN(O22)
23	=K23+L23	=K23	=L23	=M23	=LN(N23)	=LN(O23)
24	=K24+L24	=K24	=L24	=M24	=LN(N24)	=LN(O24)
25	=K25+L25	=K25	=L25	=M25	=LN(N25)	=LN(O25)
26	=K26+L26	=K26	=L26	=M26	=LN(N26)	=LN(O26)
27	=K27+L27	=K27	=L27	=M27	=LN(N27)	=LN(O27)
28	=K28+L28	=K28	=L28	=M28	=LN(N28)	=LN(O28)
29	=K29+L29	=K29	=L29	=M29	=LN(N29)	=LN(O29)
30	=K30+L30	=K30	=L30	=M30	=LN(N30)	=LN(O30)
31	=K31+L31	=K31	=L31	=M31	=LN(N31)	=LN(O31)
32	=K32+L32	=K32	=L32	=M32	=LN(N32)	=LN(O32)
33	=K33+L33	=K33	=L33	=M33	=LN(N33)	=LN(O33)
34	=K34+L34	=K34	=L34	=M34	=LN(N34)	=LN(O34)
35	=K35+L35	=K35	=L35	=M35	=LN(N35)	=LN(O35)
36	=K36+L36	=K36	=L36	=M36	=LN(N36)	=LN(O36)
37	=K37+L37	=K37	=L37	=M37	=LN(N37)	=LN(O37)
38	=K38+L38	=K38	=L38	=M38	=LN(N38)	=LN(O38)
39	=K39+L39	=K39	=L39	=M39	=LN(N39)	=LN(O39)
40					CAL PTS FOR	
41					JOINT PROBABILITY PLOT	

	S	T	U	V	W	X
1						
2						
3						
4						
5						
6						
7						
8						
9						
10						
11						
12						
13						
14						
15						
16						
17	Ordered					
18		Joint	Expected			
19		Probability	Rank		x_i^{α}	$\ln(x_i)$
20	$\ln X$	F^*	F			
21	$=LN(P21)$	$=LN(-LN(1-U21))$	$=A21/(N+1)$		$=M21^{\alpha}$	$=LN(M21)$
22	$=LN(P22)$	$=LN(-LN(1-U22))$	$=A22/(N+1)$		$=M22^{\alpha}$	$=LN(M22)$
23	$=LN(P23)$	$=LN(-LN(1-U23))$	$=A23/(N+1)$		$=M23^{\alpha}$	$=LN(M23)$
24	$=LN(P24)$	$=LN(-LN(1-U24))$	$=A24/(N+1)$		$=M24^{\alpha}$	$=LN(M^{\alpha} 4)$
25	$=LN(P25)$	$=LN(-LN(1-U25))$	$=A25/(N+1)$		$=M25^{\alpha}$	$=LN(M25)$
26	$=LN(P26)$	$=LN(-LN(1-U26))$	$=A26/(N+1)$		$=M26^{\alpha}$	$=LN(M26)$
27	$=LN(P27)$	$=LN(-LN(1-U27))$	$=A27/(N+1)$		$=M27^{\alpha}$	$=LN(M27)$
28	$=LN(P28)$	$=LN(-LN(1-U28))$	$=A28/(N+1)$		$=M28^{\alpha}$	$=LN(M28)$
29	$=LN(P29)$	$=LN(-LN(1-U29))$	$=A29/(N+1)$		$=M29^{\alpha}$	$=LN(M29)$
30	$=LN(P30)$	$=LN(-LN(1-U30))$	$=A30/(N+1)$		$=M30^{\alpha}$	$=LN(M30)$
31	$=LN(P31)$	$=LN(-LN(1-U31))$	$=A31/(N+1)$		$=M31^{\alpha}$	$=LN(M31)$
32	$=LN(P32)$	$=LN(-LN(1-U32))$	$=A32/(N+1)$		$=M32^{\alpha}$	$=LN(M32)$
33	$=LN(P33)$	$=LN(-LN(1-U33))$	$=A33/(N+1)$		$=M33^{\alpha}$	$=LN(M33)$
34	$=LN(P34)$	$=LN(-LN(1-U34))$	$=A34/(N+1)$		$=M34^{\alpha}$	$=LN(M34)$
35	$=LN(P35)$	$=LN(-LN(1-U35))$	$=A35/(N+1)$		$=M35^{\alpha}$	$=LN(M35)$
36	$=LN(P36)$	$=LN(-LN(1-U36))$	$=A36/(N+1)$		$=M36^{\alpha}$	$=LN(M36)$
37	$=LN(P37)$	$=LN(-LN(1-U37))$	$=A37/(N+1)$		$=M37^{\alpha}$	$=LN(M37)$
38	$=LN(P38)$	$=LN(-LN(1-U38))$	$=A38/(N+1)$		$=M38^{\alpha}$	$=LN(M38)$
39	$=LN(P39)$	$=LN(-LN(1-U39))$	$=A39/(N+1)$		$=M39^{\alpha}$	$=LN(M39)$
40	$=LN(beta^{*}((-LN(1-U40))^{(1/\alpha)}))$	$=LN(-LN(1-U40))$	0.00001		$=SUM(W21:W39)$	$=SUM(X21:X39)$
41	$=LN(beta^{*}((-LN(1-U41))^{(1/\alpha)}))$	$=LN(-LN(1-U41))$	0.99999			

	Y	Z
1		
2		
3		
4		
5		
6		
7		
8		
9		
10		
11		
12		
13		
14		
15		
16		
17		
18		
19	$(x_i^{\alpha}) \cdot \ln(x_i)$	
20		
21	$= (M21^{\alpha}) \cdot (\ln(M21))$	
22	$= (M22^{\alpha}) \cdot (\ln(M22))$	
23	$= (M23^{\alpha}) \cdot (\ln(M23))$	
24	$= (M24^{\alpha}) \cdot (\ln(M24))$	
25	$= (M25^{\alpha}) \cdot (\ln(M25))$	
26	$= (M26^{\alpha}) \cdot (\ln(M26))$	
27	$= (M27^{\alpha}) \cdot (\ln(M27))$	
28	$= (M28^{\alpha}) \cdot (\ln(M28))$	
29	$= (M29^{\alpha}) \cdot (\ln(M29))$	
30	$= (M30^{\alpha}) \cdot (\ln(M30))$	
31	$= (M31^{\alpha}) \cdot (\ln(M31))$	
32	$= (M32^{\alpha}) \cdot (\ln(M32))$	
33	$= (M33^{\alpha}) \cdot (\ln(M33))$	
34	$= (M34^{\alpha}) \cdot (\ln(M34))$	
35	$= (M35^{\alpha}) \cdot (\ln(M35))$	
36	$= (M36^{\alpha}) \cdot (\ln(M36))$	
37	$= (M37^{\alpha}) \cdot (\ln(M37))$	
38	$= (M38^{\alpha}) \cdot (\ln(M38))$	
39	$= (M39^{\alpha}) \cdot (\ln(M39))$	
40	$= \text{SUM}(Y21:Y39)$	$= 1/((Y40/W40) \cdot (X40/N))$
41		Iterated α

	A	B	C	D	E	F	G	H	I	J	K	L	M	N	O
1	alfa1	60		biaxialL/T	100						No. of tests	N	19.00	(entered data)	
2	beta1	100		radian	0.7854						calculated	alfa	7.28	7.2764	
3	alfa2	5		Theta	45						calculated	beta	91.72	Calc from iteration	
4	beta2	1													
5											num. sim.	MEAN	85.48		
6															
7															
8															
9															
10															
11															
12															
13															
14															
15															
16															
17															
18															
19															
20															
21	1	0.0311	0.1520	94	0.70	135.39	0	0.00	70	0.70	0	70	70	0	56
22	2	0.2993	0.0626	98	0.58	170.00	0	0.00	58	0.58	0	58	58	0	58
23	3	0.9173	0.9726	102	1.29	78.59	102	1.02	0	0.00	102	0	102	0	64
24	4	0.9528	0.3033	102	0.82	124.88	0	0.00	82	0.82	0	82	82	0	67
25	5	0.7220	0.8787	100	1.16	86.49	100	1.00	0	0.00	100	0	100	0	70
26	6	0.6049	0.3004	100	0.81	122.71	0	0.00	81	0.81	0	81	81	0	74
27	7	0.2358	0.7343	98	1.06	92.48	98	0.98	0	0.00	98	0	98	0	81
28	8	0.3298	0.5538	98	0.96	102.80	0	0.00	96	0.96	0	96	96	0	82
29	9	0.0676	0.9527	96	1.25	76.54	96	0.96	0	0.00	96	0	96	0	90
30	10	0.6099	0.1237	100	0.67	149.75	0	0.00	67	0.67	0	67	67	96	0
31	11	0.0627	0.6206	96	0.99	96.14	96	0.96	0	0.00	96	0	96	96	0
32	12	0.9884	0.6508	103	1.01	101.49	0	0.00	101	1.01	0	101	101	0	96
33	13	0.3767	0.7163	99	1.05	94.30	99	0.99	0	0.00	99	0	99	96	0
34	14	0.3750	0.4422	99	0.90	109.97	0	0.00	90	0.90	0	90	90	98	0
35	15	0.0962	0.9848	96	1.33	72.28	96	0.96	0	0.00	96	0	96	99	0
36	16	0.2309	0.1054	98	0.64	151.68	0	0.00	64	0.64	0	64	64	100	0
37	17	0.8524	0.1965	101	0.74	136.99	0	0.00	74	0.74	0	74	74	100	0
38	18	0.2614	0.0536	98	0.56	175.06	0	0.00	56	0.56	0	56	56	0	101
39	19	0.6035	0.6858	100	1.03	96.99	100	1.00	0	0.00	100	0	100	102	0
40															
41															

P	Q	R	S	T	U	V	W	X	Y	Z
1										
2										
3										
4										
5										
6										
7										
8										
9										
10										
11										
12										
13										
14										
15										
16										
17	Ordered	Ordered	Ordered		Expected					
18	Strength				Rank					
19	Vector				F					
20	X	In L	In T	In X	F*					
21	56	-6.56	4.03	4.03	-2.970	.050	2.59E+13	4.24E+00	1.10E+14	
22	58	-6.56	4.06	4.06	-2.250	100	6.64E+12	4.06E+00	2.69E+13	
23	64	-6.56	4.17	4.17	-1.817	150	3.99E+14	4.62E+00	1.84E+15	
24	67	-6.56	4.20	4.20	-1.500	200	8.13E+13	4.40E+00	3.58E+14	
25	70	-6.56	4.24	4.24	-1.246	250	3.68E+14	4.61E+00	1.70E+15	
26	74	-6.56	4.30	4.30	-1.031	300	7.99E+13	4.40E+00	3.51E+14	
27	81	-6.56	4.40	4.40	-0.842	350	3.05E+14	4.58E+00	1.40E+15	
28	82	-6.56	4.40	4.40	-0.672	400	2.62E+14	4.56E+00	1.19E+15	
29	90	-6.56	4.50	4.50	-0.514	450	2.59E+14	4.56E+00	1.18E+15	
30	96	4.56	-6.56	4.56	-0.367	500	1.88E+13	4.20E+00	7.89E+13	
31	96	4.56	-6.56	4.56	-0.225	550	2.56E+14	4.56E+00	1.17E+15	
32	96	-6.56	4.56	4.56	-0.087	600	3.85E+14	4.62E+00	1.78E+15	
33	96	4.57	-6.56	4.57	0.049	650	3.26E+14	4.59E+00	1.50E+15	
34	98	4.58	-6.56	4.58	0.186	700	1.63E+14	4.50E+00	7.34E+14	
35	99	4.59	-6.56	4.59	0.327	750	2.71E+14	4.57E+00	1.24E+15	
36	100	4.60	-6.56	4.60	0.476	800	1.47E+13	4.17E+00	6.11E+13	
37	100	4.61	-6.56	4.61	0.640	850	3.92E+13	4.30E+00	1.68E+14	
38	101	-6.56	4.62	4.62	0.834	900	5.26E+12	4.03E+00	2.12E+13	
39	102	4.62	-6.56	4.62	1.097	950	3.54E+14	4.60E+00	1.63E+15	
40		CAL PTS FOR	2.9366	-11.513	00001		3.62E+15	8.42E+01	1.65E+16	7.27644325
41		JOINT PROB	4.8546	2.443	99999				Iterated alfa	

APPENDIX D

GAUSS QUADRATURE MEAN STRENGTH INTEGRATION

A Gauss Quadrature method [Ref. 19] was used for the integration of the Expected Value mean $[\mu = \int [1-F(|S|)] ds]$ in order to find the theoretical model mean strength distribution in the stress domain for each of the seventeen (17) applied stress ratios based on a particular combination of the joint probability shape (α_1 and α_2) and scale (β_1 and β_2) parameters. The computer program was formatted in Microsoft Basic. There were two basic programs developed:

- (1) the mean integration for the applied stress ratios which were based on the normalized zero (0) through ninety (90) degree radial loading paths:

REM GAUSS QUADRATURE MEAN INTEGRATION

REM MEAN INTEGRATION FOR NORMALIZED THETA=0 TO 90

OPEN "MEAN DATA AA=" FOR OUTPUT AS #7

enter:

DIM gnums(48)

REM type gnums constants here

gnums(1) = -.9951872199970214#

gnums(2) = -.9747285559713095#

gnums(3) = -.9382745520027328#

gnums(4) = -.886415527004401#

gnums(5) = -.8200019859739029#

gnums(6) = -.7401241915785544#

gnums(7) = -.6480936519369755#

gnums(8) = -.5454214713888395#

gnums(9) = -.4337935076260451#

gnums(10) = -.3150426796961634#

gnums(11) = -.1911188674736163#

gnums(12) = -6.405689286260564D-02

FOR i = 13 TO 24 STEP 1

gnums(i) = -gnums(25-i)

NEXT i

```

gnums(25) = .0123412297999872#
gnums(26) = 2.853138862893366D-02
gnums(27) = 4.427743881741981D-02
gnums(28) = 5.929858491543678D-02
gnums(29) = .0733464814110803#
gnums(30) = 8.619016153195327D-02
gnums(31) = 9.761865210411388D-02
gnums(32) = .1074442701159656#
gnums(33) = .1155056680537256#
gnums(34) = .1216704729278034#
gnums(35) = .1258374563468283#
gnums(36) = .1279381953467522#

```

```

FOR i = 37 TO 48 STEP 1
  gnums(i)=gnums(73-i)
NEXT i

```

```

REM THETAS=NORMALIZED THETA
10 PRINT "input THETAS (in degrees)";
INPUT THETAS

```

```

IF (THETAS<0) THEN CLOSE #7
IF (THETAS<0) THEN STOP

```

```

PRINT #7,"THETAS=";THETAS

```

```

REM input limits of integration here (right > left)
PRINT "input the limits of integration (right > left)"

```

```

PRINT "input left";
INPUT left

```

```

PRINT#7,"left limit of integration=";left

```

```

PRINT"input right";
INPUT right

```

```

PRINT#7,"right limit of integration=";right

```

```

REM A1=ALFA1; A2=ALFA2; B1=BETA1; B2=BETA2
REM ALFA AND BETA ARE SHAPE AND SCALE PARAMETERS
REM RESPECTIVELY

```

```

A1=60
A2=5
B1=100

```

B2=1

REM SIGMA=SIGMA2/SIGMA1
THETAS1 = THETAS *3.141592654# / 180
SIGMA=TAN(THETAS1)*B2/B1

REM THETA=PHYSICAL THETA
THETA= ATN(SIGMA)

c1 = -(left + right) / (right - left)
c2 = .5 * (right - left)

ANSWER= 0

REM FUNCTION TO BE INTEGRATED
FOR i = 1 TO 24
 X = (gnums(i) - c1)*c2
 F = EXP(-((X*COS(THETA)/B1)^A1 + (X*SIN(THETA)/B2)^A2))
 ANSWER = ANSWER + gnums(i+24) * F
NEXT i

ANSWER = ANSWER * c2

PRINT "ANSWER = ";ANSWER
PRINT
PRINT #7,"ANSWER=";ANSWER
PRINT #7," "

GOTO 10
END

- (2) the mean integration for the applied stress ratios which were based only on the normalized (uniaxial) zero (0) and ninety (90) degree radial loading paths:

REM GAUSS QUADRATURE MEAN INTEGRATION

REM MEAN INTEGRATION FOR NORMALIZED THETA=0 AND 90 ONLY

OPEN "MEAN DATA A=" FOR OUTPUT AS #7
enter:
DIM gnums(48)
REM type gnums constants here
gnums(1) = -.9951872199970214#
gnums(2) = -.9747285559713095#

```

gnums(3) = -.9382745520027328#
gnums(4) = -.886415527004401#
gnums(5) = -.8200019859739029#
gnums(6) = -.7401241915785544#
gnums(7) = -.6480936519369755#
gnums(8) = -.5454214713888395#
gnums(9) = -.4337935076260451#
gnums(10) = -.3150426796961634#
gnums(11) = -.1911188674736163#
gnums(12) = -6.405689286260564D-02

```

```

FOR i = 13 TO 24 STEP 1
  gnums(i) = -gnums(25-i)
NEXT i

```

```

gnums(25) = .0123412297999872#
gnums(26) = 2.853138862893366D-02
gnums(27) = 4.427743881741981D-02
gnums(28) = 5.929858491543678D-02
gnums(29) = .0733464814110803#
gnums(30) = 8.619016153195327D-02
gnums(31) = 9.761865210411388D-02
gnums(32) = .1074442701159656#
gnums(33) = .1155056680537256#
gnums(34) = .1216704729278034#
gnums(35) = .1258374563468283#
gnums(36) = .1279381953467522#

```

```

FOR i = 37 TO 48 STEP 1
  gnums(i) = gnums(73-i)
NEXT i

```

```

REM THETAS=THETA NORMALIZED
10 PRINT "input THETAS (in degrees)";
INPUT THETAS

```

```

IF (THETAS<0) THEN CLOSE #7
IF (THETAS<0) THEN STOP

```

```

PRINT #7,"THETAS=";THETAS

```

```

REM input limits of integration here (right > left)
PRINT "input the limits of integration (right > left)"

```

```

PRINT "input left";
INPUT left

```

```

PRINT#7,"left limit of integration=";left

PRINT"input right";
INPUT right

PRINT#7,"right limit of integration=";right

REM A1=ALFA1; A2=ALFA2; B1=BETA1; B2=BETA2
REM ALFA AND BETA ARE SHAPE AND SCALE PARAMETERS
REM RESPECTIVELY

A1=60
A2=5
B1=100
B2=1

REM THETAS1=PHYSICAL THETA
THETAS1 = THETAS *3.141592654# / 180

c1 = -(left + right) / (right - left)
c2 = .5 * (right - left)

ANSWER= 0

REM FUNCTION TO BE INTEGRATED
FOR i = 1 TO 24
    X = (gnums(i) - c1)*c2
    F = EXP(-((X*COS(THETAS1)/B1)^A1 + (X*SIN(THETAS1)/B2)^A2))
    ANSWER = ANSWER + gnums(i+24) * F
NEXT i

ANSWER = ANSWER * c2

PRINT "ANSWER = ";ANSWER
PRINT
PRINT #7,"ANSWER=";ANSWER
PRINT #7," "

GOTO 10
END

```

APPENDIX E

SIMULATION/MODEL MEAN STRENGTH WORKSHEET

This particular worksheet exhibited the formulation of the mean strength failure envelopes or failure surfaces in the stress domain as defined by the failure criteria for both cases. For the biaxial L/T numerical simulation and the theoretical mathematical model, the failure envelope or failure surface was defined as:

- (1) the mean strength distribution or contour of the seventeen (17) applied stress ratios for a particular sample size and a particular shape parameter (α_1 and α_2) combination with the mean strength distribution or contour normalized by the joint probability function (uniaxial) scale parameters (β_1 and β_2).
- (2) the mean strength distribution or contour of the seventeen (17) applied stress ratios for a particular sample size and a particular shape parameter (α_1 and α_2) combination with the mean strength distribution or contour normalized by the mean strength at the normalized (uniaxial) zero (0) degree and ninety (90) degree radial loading paths (transformed theta) respectively.

A mathematical mean function based on the uniaxial longitudinal and transverse scale (β) and shape (α) parameters and the Gamma function was used at the normalized (uniaxial) zero (0) degree and ninety (90) degree radial loading paths for correlation of the numerical simulation and theoretical model mean strengths at the respective radial loading paths. The mathematical mean function was defined as: $\mu = \beta\Gamma(1 + 1/\alpha)$ [Ref. 20].

	A	B	C	D
1	BETA1	=100		
2	BETA2	=1		
3	ALFA1	=60		
4	ALFA2	=5		
5	alfa and beta are the joint			
6	probability shape and scale			
7	parameters respectively.			
8				
9				
10		NUMERICAL	THEORETICAL	GAMMA
11	NORMALIZED	SIMULATED	MODEL	FUNCTION
12	THETA	MEAN	MEAN	COMPUTED
13	0			MEAN
14	10			=BETA1*0.9904745
15	20			
16	30			
17	35			
18	39			
19	42			
20	44			
21	45			
22	46			
23	48			
24	51			
25	55			
26	60			
27	70			
28	80			
29	90			=BETA2*0.9181687

	E	F	G
1			
2			
3		The numerical simulation mean strength was based on	
4		the biaxial L/T numerical simulation.	
5			
6			
7		The theoretical model mean strength was based on	
8		the Gauss Quadrature integration method.	
9			
10			
11			
12			
13			
14			
15			
16			
17			
18			
19			
20			
21			
22			
23			
24			
25			
26			
27			
28			
29			

	H	I	J
1			
2		U=mean strength	
3			
4			
5			
6			
7			
8			
9			
10	physical		
11	NON-NORMALIZED		
12	THETA	U*COS()	U*SIN()
13	=ATAN(TAN(\$A13*3.141592654/180)*BETA2/BETA1)	=B13*COS(\$H13)	=B13*SIN(\$H13)
14	=ATAN(TAN(\$A14*3.141592654/180)*BETA2/BETA1)	=B14*COS(\$H14)	=B14*SIN(\$H14)
15	=ATAN(TAN(\$A15*3.141592654/180)*BETA2/BETA1)	=B15*COS(\$H15)	=B15*SIN(\$H15)
16	=ATAN(TAN(\$A16*3.141592654/180)*BETA2/BETA1)	=B16*COS(\$H16)	=B16*SIN(\$H16)
17	=ATAN(TAN(\$A17*3.141592654/180)*BETA2/BETA1)	=B17*COS(\$H17)	=B17*SIN(\$H17)
18	=ATAN(TAN(\$A18*3.141592654/180)*BETA2/BETA1)	=B18*COS(\$H18)	=B18*SIN(\$H18)
19	=ATAN(TAN(\$A19*3.141592654/180)*BETA2/BETA1)	=B19*COS(\$H19)	=B19*SIN(\$H19)
20	=ATAN(TAN(\$A20*3.141592654/180)*BETA2/BETA1)	=B20*COS(\$H20)	=B20*SIN(\$H20)
21	=ATAN(TAN(\$A21*3.141592654/180)*BETA2/BETA1)	=B21*COS(\$H21)	=B21*SIN(\$H21)
22	=ATAN(TAN(\$A22*3.141592654/180)*BETA2/BETA1)	=B22*COS(\$H22)	=B22*SIN(\$H22)
23	=ATAN(TAN(\$A23*3.141592654/180)*BETA2/BETA1)	=B23*COS(\$H23)	=B23*SIN(\$H23)
24	=ATAN(TAN(\$A24*3.141592654/180)*BETA2/BETA1)	=B24*COS(\$H24)	=B24*SIN(\$H24)
25	=ATAN(TAN(\$A25*3.141592654/180)*BETA2/BETA1)	=B25*COS(\$H25)	=B25*SIN(\$H25)
26	=ATAN(TAN(\$A26*3.141592654/180)*BETA2/BETA1)	=B26*COS(\$H26)	=B26*SIN(\$H26)
27	=ATAN(TAN(\$A27*3.141592654/180)*BETA2/BETA1)	=B27*COS(\$H27)	=B27*SIN(\$H27)
28	=ATAN(TAN(\$A28*3.141592654/180)*BETA2/BETA1)	=B28*COS(\$H28)	=B28*SIN(\$H28)
29	=ATAN(TAN(\$A29*3.141592654/180)*BETA2/BETA1)	=B29*COS(\$H29)	=B29*SIN(\$H29)

	K	L	M	N
1	SIMULATED	MEAN		
2	U(0)	=\$B13		
3	U(90)	=\$B29		
4				
5	NUMERICAL	SIMULATION		
6				
7	failure envelopes as defined			
8	by the numerical simulation			
9	failure criteria			
10				
11				
12	U*COS(J)/B1	U*SIN(J)/B2	SIGMA1/U(0)	SIGMA2/U(90)
13	=\$I13/BETA1	=\$J13/BETA2	=\$I13/U(0)	=\$J13/U(90)
14	=\$I14/BETA1	=\$J14/BETA2	=\$I14/U(0)	=\$J14/U(90)
15	=\$I15/BETA1	=\$J15/BETA2	=\$I15/U(0)	=\$J15/U(90)
16	=\$I16/BETA1	=\$J16/BETA2	=\$I16/U(0)	=\$J16/U(90)
17	=\$I17/BETA1	=\$J17/BETA2	=\$I17/U(0)	=\$J17/U(90)
18	=\$I18/BETA1	=\$J18/BETA2	=\$I18/U(0)	=\$J18/U(90)
19	=\$I19/BETA1	=\$J19/BETA2	=\$I19/U(0)	=\$J19/U(90)
20	=\$I20/BETA1	=\$J20/BETA2	=\$I20/U(0)	=\$J20/U(90)
21	=\$I21/BETA1	=\$J21/BETA2	=\$I21/U(0)	=\$J21/U(90)
22	=\$I22/BETA1	=\$J22/BETA2	=\$I22/U(0)	=\$J22/U(90)
23	=\$I23/BETA1	=\$J23/BETA2	=\$I23/U(0)	=\$J23/U(90)
24	=\$I24/BETA1	=\$J24/BETA2	=\$I24/U(0)	=\$J24/U(90)
25	=\$I25/BETA1	=\$J25/BETA2	=\$I25/U(0)	=\$J25/U(90)
26	=\$I26/BETA1	=\$J26/BETA2	=\$I26/U(0)	=\$J26/U(90)
27	=\$I27/BETA1	=\$J27/BETA2	=\$I27/U(0)	=\$J27/U(90)
28	=\$I28/BETA1	=\$J28/BETA2	=\$I28/U(0)	=\$J28/U(90)
29	=\$I29/BETA1	=\$J29/BETA2	=\$I29/U(0)	=\$J29/U(90)

	O	P	Q	R
1				THEORETICAL
2		U=mean strength		U(0)
3				U(90)
4				
5				THEORETICAL
6				
7				failure envelopes as defined
8				by the theoretical model
9				failure criteria
10				
11				
12		U*COS()	U*SIN()	U*COS()/B1
13		=C13*COS(\$H13)	=C13*SIN(\$H13)	=P13/BETA1
14		=C14*COS(\$H14)	=C14*SIN(\$H14)	=P14/BETA1
15		=C15*COS(\$H15)	=C15*SIN(\$H15)	=P15/BETA1
16		=C16*COS(\$H16)	=C16*SIN(\$H16)	=P16/BETA1
17		=C17*COS(\$H17)	=C17*SIN(\$H17)	=P17/BETA1
18		=C18*COS(\$H18)	=C18*SIN(\$H18)	=P18/BETA1
19		=C19*COS(\$H19)	=C19*SIN(\$H19)	=P19/BETA1
20		=C20*COS(\$H20)	=C20*SIN(\$H20)	=P20/BETA1
21		=C21*COS(\$H21)	=C21*SIN(\$H21)	=P21/BETA1
22		=C22*COS(\$H22)	=C22*SIN(\$H22)	=P22/BETA1
23		=C23*COS(\$H23)	=C23*SIN(\$H23)	=P23/BETA1
24		=C24*COS(\$H24)	=C24*SIN(\$H24)	=P24/BETA1
25		=C25*COS(\$H25)	=C25*SIN(\$H25)	=P25/BETA1
26		=C26*COS(\$H26)	=C26*SIN(\$H26)	=P26/BETA1
27		=C27*COS(\$H27)	=C27*SIN(\$H27)	=P27/BETA1
28		=C28*COS(\$H28)	=C28*SIN(\$H28)	=P28/BETA1
29		=C29*COS(\$H29)	=C29*SIN(\$H29)	=P29/BETA1

	S	T	U
1	MEAN		
2	=\$C13		
3	=\$C29		
4			
5	MODEL		
6			
7			
8			
9			
10			
11			
12	U*SIN()/B2	SIGMA1/U(0)	SIGMA2/U(90)
13	=\$Q13/BETA2	=\$P13/U(0)	=\$Q13/U(90)
14	=\$Q14/BETA2	=\$P14/U(0)	=\$Q14/U(90)
15	=\$Q15/BETA2	=\$P15/U(0)	=\$Q15/U(90)
16	=\$Q16/BETA2	=\$P16/U(0)	=\$Q16/U(90)
17	=\$Q17/BETA2	=\$P17/U(0)	=\$Q17/U(90)
18	=\$Q18/BETA2	=\$P18/U(0)	=\$Q18/U(90)
19	=\$Q19/BETA2	=\$P19/U(0)	=\$Q19/U(90)
20	=\$Q20/BETA2	=\$P20/U(0)	=\$Q20/U(90)
21	=\$Q21/BETA2	=\$P21/U(0)	=\$Q21/U(90)
22	=\$Q22/BETA2	=\$P22/U(0)	=\$Q22/U(90)
23	=\$Q23/BETA2	=\$P23/U(0)	=\$Q23/U(90)
24	=\$Q24/BETA2	=\$P24/U(0)	=\$Q24/U(90)
25	=\$Q25/BETA2	=\$P25/U(0)	=\$Q25/U(90)
26	=\$Q26/BETA2	=\$P26/U(0)	=\$Q26/U(90)
27	=\$Q27/BETA2	=\$P27/U(0)	=\$Q27/U(90)
28	=\$Q28/BETA2	=\$P28/U(0)	=\$Q28/U(90)
29	=\$Q29/BETA2	=\$P29/U(0)	=\$Q29/U(90)

APPENDIX F

RELIABILITY/FAILURE FUNCTION WORKSHEET

This particular worksheet exhibited the formulation of the joint probability reliability and failure functions based on a applied stress ratio and a particular combination of the joint probability shape (α_1 and α_2) and scale (β_1 and β_2) parameters.

	A	B
1	alpha1	=60
2	beta1	=100
3	alpha2	=5
4	beta2	=1
5		alfa and beta are the joint probability shape and scale parameters respectively
6		
7		THEORETICAL MODEL
8	STRENGTH	RELIABILITY
9	VECTOR	FUNCTION
10	S	R(S)
11	=0	$= \text{EXP}(-((A11 * (\cos(\text{THETA}))/\text{beta1})^{\text{alpha1}} + (A11 * (\sin(\text{THETA}))/\text{beta2})^{\text{alpha2}}))$
12	=\$A11+1	$= \text{EXP}(-((A12 * (\cos(\text{THETA}))/\text{beta1})^{\text{alpha1}} + (A12 * (\sin(\text{THETA}))/\text{beta2})^{\text{alpha2}}))$
13	=\$A12+1	$= \text{EXP}(-((A13 * (\cos(\text{THETA}))/\text{beta1})^{\text{alpha1}} + (A13 * (\sin(\text{THETA}))/\text{beta2})^{\text{alpha2}}))$
14	=\$A13+1	$= \text{EXP}(-((A14 * (\cos(\text{THETA}))/\text{beta1})^{\text{alpha1}} + (A14 * (\sin(\text{THETA}))/\text{beta2})^{\text{alpha2}}))$
15	=\$A14+1	$= \text{EXP}(-((A15 * (\cos(\text{THETA}))/\text{beta1})^{\text{alpha1}} + (A15 * (\sin(\text{THETA}))/\text{beta2})^{\text{alpha2}}))$
16	=\$A15+1	$= \text{EXP}(-((A16 * (\cos(\text{THETA}))/\text{beta1})^{\text{alpha1}} + (A16 * (\sin(\text{THETA}))/\text{beta2})^{\text{alpha2}}))$
17	=\$A16+1	$= \text{EXP}(-((A17 * (\cos(\text{THETA}))/\text{beta1})^{\text{alpha1}} + (A17 * (\sin(\text{THETA}))/\text{beta2})^{\text{alpha2}}))$
18	=\$A17+1	$= \text{EXP}(-((A18 * (\cos(\text{THETA}))/\text{beta1})^{\text{alpha1}} + (A18 * (\sin(\text{THETA}))/\text{beta2})^{\text{alpha2}}))$
19	=\$A18+1	$= \text{EXP}(-((A19 * (\cos(\text{THETA}))/\text{beta1})^{\text{alpha1}} + (A19 * (\sin(\text{THETA}))/\text{beta2})^{\text{alpha2}}))$
20	=\$A19+1	$= \text{EXP}(-((A20 * (\cos(\text{THETA}))/\text{beta1})^{\text{alpha1}} + (A20 * (\sin(\text{THETA}))/\text{beta2})^{\text{alpha2}}))$
21	=\$A20+1	$= \text{EXP}(-((A21 * (\cos(\text{THETA}))/\text{beta1})^{\text{alpha1}} + (A21 * (\sin(\text{THETA}))/\text{beta2})^{\text{alpha2}}))$
22	=\$A21+1	$= \text{EXP}(-((A22 * (\cos(\text{THETA}))/\text{beta1})^{\text{alpha1}} + (A22 * (\sin(\text{THETA}))/\text{beta2})^{\text{alpha2}}))$
23	=\$A22+1	$= \text{EXP}(-((A23 * (\cos(\text{THETA}))/\text{beta1})^{\text{alpha1}} + (A23 * (\sin(\text{THETA}))/\text{beta2})^{\text{alpha2}}))$
24	=\$A23+1	$= \text{EXP}(-((A24 * (\cos(\text{THETA}))/\text{beta1})^{\text{alpha1}} + (A24 * (\sin(\text{THETA}))/\text{beta2})^{\text{alpha2}}))$
25	=\$A24+1	$= \text{EXP}(-((A25 * (\cos(\text{THETA}))/\text{beta1})^{\text{alpha1}} + (A25 * (\sin(\text{THETA}))/\text{beta2})^{\text{alpha2}}))$
26	=\$A25+1	$= \text{EXP}(-((A26 * (\cos(\text{THETA}))/\text{beta1})^{\text{alpha1}} + (A26 * (\sin(\text{THETA}))/\text{beta2})^{\text{alpha2}}))$
27	=\$A26+1	$= \text{EXP}(-((A27 * (\cos(\text{THETA}))/\text{beta1})^{\text{alpha1}} + (A27 * (\sin(\text{THETA}))/\text{beta2})^{\text{alpha2}}))$
28	=\$A27+1	$= \text{EXP}(-((A28 * (\cos(\text{THETA}))/\text{beta1})^{\text{alpha1}} + (A28 * (\sin(\text{THETA}))/\text{beta2})^{\text{alpha2}}))$
29	=\$A28+1	$= \text{EXP}(-((A29 * (\cos(\text{THETA}))/\text{beta1})^{\text{alpha1}} + (A29 * (\sin(\text{THETA}))/\text{beta2})^{\text{alpha2}}))$
30	=\$A29+1	$= \text{EXP}(-((A30 * (\cos(\text{THETA}))/\text{beta1})^{\text{alpha1}} + (A30 * (\sin(\text{THETA}))/\text{beta2})^{\text{alpha2}}))$
31	=\$A30+1	$= \text{EXP}(-((A31 * (\cos(\text{THETA}))/\text{beta1})^{\text{alpha1}} + (A31 * (\sin(\text{THETA}))/\text{beta2})^{\text{alpha2}}))$
32	=\$A31+1	$= \text{EXP}(-((A32 * (\cos(\text{THETA}))/\text{beta1})^{\text{alpha1}} + (A32 * (\sin(\text{THETA}))/\text{beta2})^{\text{alpha2}}))$

	C		D
1	PHYSICAL	THETA	
2			
3			
4		SIG2SIG1	
5		radians	
6	NORMALIZED	THETA1	
7			
8			
9			
10	R1(S)	R2(S)	
11	=EXP(-(\$A11*COS(THETA)/beta1)^alpha1))	=EXP(-(\$A11*SIN(THETA)/beta2)^alpha2))	
12	=EXP(-(\$A12*COS(THETA)/beta1)^alpha1))	=EXP(-(\$A12*SIN(THETA)/beta2)^alpha2))	
13	=EXP(-(\$A13*COS(THETA)/beta1)^alpha1))	=EXP(-(\$A13*SIN(THETA)/beta2)^alpha2))	
14	=EXP(-(\$A14*COS(THETA)/beta1)^alpha1))	=EXP(-(\$A14*SIN(THETA)/beta2)^alpha2))	
15	=EXP(-(\$A15*COS(THETA)/beta1)^alpha1))	=EXP(-(\$A15*SIN(THETA)/beta2)^alpha2))	
16	=EXP(-(\$A16*COS(THETA)/beta1)^alpha1))	=EXP(-(\$A16*SIN(THETA)/beta2)^alpha2))	
17	=EXP(-(\$A17*COS(THETA)/beta1)^alpha1))	=EXP(-(\$A17*SIN(THETA)/beta2)^alpha2))	
18	=EXP(-(\$A18*COS(THETA)/beta1)^alpha1))	=EXP(-(\$A18*SIN(THETA)/beta2)^alpha2))	
19	=EXP(-(\$A19*COS(THETA)/beta1)^alpha1))	=EXP(-(\$A19*SIN(THETA)/beta2)^alpha2))	
20	=EXP(-(\$A20*COS(THETA)/beta1)^alpha1))	=EXP(-(\$A20*SIN(THETA)/beta2)^alpha2))	
21	=EXP(-(\$A21*COS(THETA)/beta1)^alpha1))	=EXP(-(\$A21*SIN(THETA)/beta2)^alpha2))	
22	=EXP(-(\$A22*COS(THETA)/beta1)^alpha1))	=EXP(-(\$A22*SIN(THETA)/beta2)^alpha2))	
23	=EXP(-(\$A23*COS(THETA)/beta1)^alpha1))	=EXP(-(\$A23*SIN(THETA)/beta2)^alpha2))	
24	=EXP(-(\$A24*COS(THETA)/beta1)^alpha1))	=EXP(-(\$A24*SIN(THETA)/beta2)^alpha2))	
25	=EXP(-(\$A25*COS(THETA)/beta1)^alpha1))	=EXP(-(\$A25*SIN(THETA)/beta2)^alpha2))	
26	=EXP(-(\$A26*COS(THETA)/beta1)^alpha1))	=EXP(-(\$A26*SIN(THETA)/beta2)^alpha2))	
27	=EXP(-(\$A27*COS(THETA)/beta1)^alpha1))	=EXP(-(\$A27*SIN(THETA)/beta2)^alpha2))	
28	=EXP(-(\$A28*COS(THETA)/beta1)^alpha1))	=EXP(-(\$A28*SIN(THETA)/beta2)^alpha2))	
29	=EXP(-(\$A29*COS(THETA)/beta1)^alpha1))	=EXP(-(\$A29*SIN(THETA)/beta2)^alpha2))	
30	=EXP(-(\$A30*COS(THETA)/beta1)^alpha1))	=EXP(-(\$A30*SIN(THETA)/beta2)^alpha2))	
31	=EXP(-(\$A31*COS(THETA)/beta1)^alpha1))	=EXP(-(\$A31*SIN(THETA)/beta2)^alpha2))	
32	=EXP(-(\$A32*COS(THETA)/beta1)^alpha1))	=EXP(-(\$A32*SIN(THETA)/beta2)^alpha2))	

	E	F	G
1	=ATAN(SIG2SIG1)		
2			
3			
4	=TAN(radians)*beta2/beta1		
5	=3.141592654/180*THETA1		
6	45		
7			
8	THEORETICAL MODEL		
9	FAILURE FUNCTION		
10	F(S)	F1(S)	F2(S)
11	=1-\$B11	=1-\$C11	=1-\$D11
12	=1-\$B12	=1-\$C12	=1-\$D12
13	=1-\$B13	=1-\$C13	=1-\$D13
14	=1-\$B14	=1-\$C14	=1-\$D14
15	=1-\$B15	=1-\$C15	=1-\$D15
16	=1-\$B16	=1-\$C16	=1-\$D16
17	=1-\$B17	=1-\$C17	=1-\$D17
18	=1-\$B18	=1-\$C18	=1-\$D18
19	=1-\$B19	=1-\$C19	=1-\$D19
20	=1-\$B20	=1-\$C20	=1-\$D20
21	=1-\$B21	=1-\$C21	=1-\$D21
22	=1-\$B22	=1-\$C22	=1-\$D22
23	=1-\$B23	=1-\$C23	=1-\$D23
24	=1-\$B24	=1-\$C24	=1-\$D24
25	=1-\$B25	=1-\$C25	=1-\$D25
26	=1-\$B26	=1-\$C26	=1-\$D26
27	=1-\$B27	=1-\$C27	=1-\$D27
28	=1-\$B28	=1-\$C28	=1-\$D28
29	=1-\$B29	=1-\$C29	=1-\$D29
30	=1-\$B30	=1-\$C30	=1-\$D30
31	=1-\$B31	=1-\$C31	=1-\$D31
32	=1-\$B32	=1-\$C32	=1-\$D32

APPENDIX G

PERCENTILE STRENGTH WORKSHEET

This particular worksheet exhibited the formulation of the percentile strength failure envelopes or failure surfaces in the stress domain as defined by the theoretical model failure criteria. The percentile failure contour was obtained at the different combined stress levels by assigning $F(|S|)$ a constant percentile (i.e., $F(|S|) = 0.10$ for the ten (10) percentile contour) and solving for $(|S|)$ by iteration. This iteration was repeated for the seventeen (17) applied stress ratios for a particular combination of the joint probability shape parameters (α_1 and α_2).

	A	B
1	alfa and beta are the joint	alfa1
2	probability shape and scale	alfa2
3	parameters respectively	beta1
4		beta2
5		
6	S is the strength vector	
7		
8	old S	=\$B9
9	new S	=B8*(1-converge*(C8-aim)/MAX(aim,C8))
10		
11	aim	0.1
12	converge	0.1
13		
14		
15		
16		
17		
18		
19		
20		
21		
22		
23		
24		
25		
26		
27		

	C	D
1	60	
2	5	
3	100	
4	1	
5		
6	theoretical model failure function	
7	$F(S)$	
8	$= 1 - \text{EXP}(-(B8 \cdot \text{COS}(\theta) / \beta_1)^\alpha + (B8 \cdot \text{SIN}(\theta) / \beta_2)^\alpha)$	
9		
10		
11	percentile aim point	
12		
13		
14		
15		
16		
17		
18		
19		
20		
21		
22		
23		
24		
25		
26		
27		

	E	F
1		columns A to F is the iterate process to determine the
2		percentile strength for a particular applied stress
3		ratio and a particular joint shape and scale
4		combination and a particular percentile.
5	physical	
6	non-normalized	
7	theta	=ATAN(TAN(\$F10*3.141592654/180)*beta2/beta1)
8		
9	normalized	
10	theta1	45
11		
12		
13		
14		
15		
16		
17		
18		
19		
20		
21		
22		
23		
24		
25		
26		
27		

	G	H	I
1			
2			
3			
4			
5			S
6		normalized	percentile
7		theta	strength
8			$F(s) = .100$
9			
10			
11		0	
12		10	
13		20	
14		30	
15		35	
16		39	
17		42	
18		44	
19		45	
20		46	
21		48	
22		51	
23		55	
24		60	
25		70	
26		80	
27		90	

	J	K
1		
2		
3		
4		
5	S	
6	percentile	physical
7	strength	non-normalized
8	F(S)=.900	theta
9		
10		
11		=ATAN(TAN(\$H11*3.141592654/180)*beta2/beta1)
12		=ATAN(TAN(\$H12*3.141592654/180)*beta2/beta1)
13		=ATAN(TAN(\$H13*3.141592654/180)*beta2/beta1)
14		=ATAN(TAN(\$H14*3.141592654/180)*beta2/beta1)
15		=ATAN(TAN(\$H15*3.141592654/180)*beta2/beta1)
16		=ATAN(TAN(\$H16*3.141592654/180)*beta2/beta1)
17		=ATAN(TAN(\$H17*3.141592654/180)*beta2/beta1)
18		=ATAN(TAN(\$H18*3.141592654/180)*beta2/beta1)
19		=ATAN(TAN(\$H19*3.141592654/180)*beta2/beta1)
20		=ATAN(TAN(\$H20*3.141592654/180)*beta2/beta1)
21		=ATAN(TAN(\$H21*3.141592654/180)*beta2/beta1)
22		=ATAN(TAN(\$H22*3.141592654/180)*beta2/beta1)
23		=ATAN(TAN(\$H23*3.141592654/180)*beta2/beta1)
24		=ATAN(TAN(\$H24*3.141592654/180)*beta2/beta1)
25		=ATAN(TAN(\$H25*3.141592654/180)*beta2/beta1)
26		=ATAN(TAN(\$H26*3.141592654/180)*beta2/beta1)
27		=ATAN(TAN(\$H27*3.141592654/180)*beta2/beta1)

	L	M	N
1			columns N and O define the
2			percentile strength
3			distribution based on the
4			theoretical model failure
5			criteria
6			
7			
8			
9			
10	S*COS()	S*SIN()	S*COS()/B1
11	=\$I11*COS(\$K11)	=\$I11*SIN(\$K11)	=\$L11/beta1
12	=\$I12*COS(\$K12)	=\$I12*SIN(\$K12)	=\$L12/beta1
13	=\$I13*COS(\$K13)	=\$I13*SIN(\$K13)	=\$L13/beta1
14	=\$I14*COS(\$K14)	=\$I14*SIN(\$K14)	=\$L14/beta1
15	=\$I15*COS(\$K15)	=\$I15*SIN(\$K15)	=\$L15/beta1
16	=\$I16*COS(\$K16)	=\$I16*SIN(\$K16)	=\$L16/beta1
17	=\$I17*COS(\$K17)	=\$I17*SIN(\$K17)	=\$L17/beta1
18	=\$I18*COS(\$K18)	=\$I18*SIN(\$K18)	=\$L18/beta1
19	=\$I19*COS(\$K19)	=\$I19*SIN(\$K19)	=\$L19/beta1
20	=\$I20*COS(\$K20)	=\$I20*SIN(\$K20)	=\$L20/beta1
21	=\$I21*COS(\$K21)	=\$I21*SIN(\$K21)	=\$L21/beta1
22	=\$I22*COS(\$K22)	=\$I22*SIN(\$K22)	=\$L22/beta1
23	=\$I23*COS(\$K23)	=\$I23*SIN(\$K23)	=\$L23/beta1
24	=\$I24*COS(\$K24)	=\$I24*SIN(\$K24)	=\$L24/beta1
25	=\$I25*COS(\$K25)	=\$I25*SIN(\$K25)	=\$L25/beta1
26	=\$I26*COS(\$K26)	=\$I26*SIN(\$K26)	=\$L26/beta1
27	=\$I27*COS(\$K27)	=\$I27*SIN(\$K27)	=\$L27/beta1

	0
1	
2	
3	
4	
5	
6	
7	
8	
9	
10	S*SIN()/B2
11	= \$M11/beta2
12	= \$M12/beta2
13	= \$M13/beta2
14	= \$M14/beta2
15	= \$M15/beta2
16	= \$M16/beta2
17	= \$M17/beta2
18	= \$M18/beta2
19	= \$M19/beta2
20	= \$M20/beta2
21	= \$M21/beta2
22	= \$M22/beta2
23	= \$M23/beta2
24	= \$M24/beta2
25	= \$M25/beta2
26	= \$M26/beta2
27	= \$M27/beta2

LIST OF REFERENCES

1. Wu, Edward M., "AE 3101 Class Notes," Naval Postgraduate School, Monterey, California, October 1987.
2. Wu, Edward M., "AE 3101 Class Notes," Naval Postgraduate School, Monterey, California, October 1987.
3. Tsai, Stephen W., Composites Design, Think Composites, Dayton, Ohio, pp. 1.4 and 29.1-29.20, Third Edition.
4. Jones, Robert M., Mechanics of Composite Materials, Hemisphere Publishing Corporation, New York, p.14, 1975.
5. Wu, Edward M., "Phenomenological Anisotropic Failure Criterion," in Composite Materials, ed. L. J. Broutman and R. H. Krock, Academic Press, Inc., New York, vol.II pp. 353-431, 1974.
6. Tsai, Stephen W., Composites Design, Think Composites, Dayton, Ohio, pp. 29.1-29.20, Third Edition.
7. Wu, Edward M., "Phenomenological Anisotropic Failure Criterion," in Composite Materials, ed. L. J. Broutman and R. H. Krock, Academic Press, Inc., New York, vol.II pp. 353-431, 1974.
8. Tsai, Stephen W., Composites Design, Think Composites, Dayton, Ohio, pp. 29.1-29.20, Third Edition.
9. Wu, Edward M., "Phenomenological Anisotropic Failure Criterion," in Composite Materials, ed. L. J. Broutman and R. H. Krock, Academic Press, Inc., New York, vol.II pp. 353-431, 1974.
10. Tsai, Stephen W., Composites Design, Think Composites, Dayton, Ohio, pp. 29.1-29.20, Third Edition.
11. Wu, Edward M., "Failure Criteria for Anisotropic Solids Lecture at UCLA," Naval Postgraduate School, Monterey, California, March 1987.
12. Wu, Edward M., "AE 4202 Class Notes," Naval Postgraduate School, Monterey, California, January 1987.
13. Wu, Edward M., "AE 4202 Class Notes," Naval Postgraduate School, Monterey, California, January 1987.
14. Wu, Edward M., "AE 4202 Class Notes," Naval Postgraduate School, Monterey, California, January 1987.

15. Wu, Edward M., "AE 4202 Class Notes," Naval Postgraduate School, Monterey, California, January 1987.
16. Wu, Edward M., "Failure Criteria for Anisotropic Solids Lecture at UCLA," Naval Postgraduate School, Monterey, California, March 1987.
17. Wu, Edward M., "Failure Criteria for Anisotropic Solids Lecture at UCLA," Naval Postgraduate School, Monterey, California, March 1987.
18. Nelson, K. J., Private Communication with Professor Edward M. Wu, Naval Postgraduate School, Monterey, California, July 1987.
19. Davis, Philip J. and Polonsky, Ivan, "Numerical Interpolation, Differentiation, and Integration," in Handbook of Mathematical Functions with Formulas, Graphs, and Mathematical Tables, ed. M. Abramowitz and I. A. Stegun, National Bureau of Standards, John Wiley & Sons, Inc., pp. 875 and 887-916, 1972.
20. Wu, Edward M., "AE 4202 Class Notes," Naval Postgraduate School, Monterey, California, January 1987.

BIBLIOGRAPHY

Jones, Robert M., Mechanics of Composite Materials, Hemisphere Publishing Corporation, New York, 1975.

Smith, Charles O., Introduction to Reliability in Design, Robert E. Krieger Publishing Co., Malabar, Florida, 1986.

Tsai, Stephen W., Composites Design, Think Composites, Dayton, Ohio, Third Edition.

Wu, Edward M., "Phenomenological Anisotropic Failure Criterion," in Composite Materials, ed. L. J. Broutman and R. H. Krock, Academic Press, Inc., New York, vol.II, 1974.

INITIAL DISTRIBUTION LIST

		<u>No. Copies</u>
1.	Commander, Naval Air Systems Command Assistant Commander for Systems & Engineering (NAIR-05) 1421 Jefferson Davis Highway (JP-2) Arlington, VA 22202	1
2.	Dr. Robert Badalian Chief, Mechanics of Materials Branch Code 6380 Naval Research Laboratory Washington, D.C. 20375	1
3.	Defense Technical Information Center Cameron Station Alexandria, VA 22304-6145	2
4.	Library, Code 0142 Naval Postgraduate School Monterey, CA 93943-5002	2
5.	Dr. Edward M. Wu, Code 67wt Professor of Aeronautics Naval Postgraduate School Monterey, CA 93942-5000	10
6.	Kenneth J. Nelson, LCDR,USN Commander, Naval Air Force, U.S. Atlantic Fleet Code: 527 Norfolk, VA 23511-5188	3

END

DATE

FILMED

DTIC

JULY 88